

1 **ALG-2 interacting protein-X (Alix) is required for activity-dependent bulk** 2 **endocytosis at brain synapses**

3
4 Marine H. Laporte ^{1,2,*}, Kwang Il Chi ^{1*}, Marta Rolland ¹, Laura C. Caudal ³, José Martinez-
5 Hernandez ^{1,4}, Magalie Martineau ⁵, Christine Chatellard ^{1,6} Eric Denarier ¹, Vincent Mercier ^{1,7},
6 Florent Lemaître ^{1,8}, Béatrice Blot ¹, Eve Moutaux ¹, Maxime Cazorla ¹, Alain Buisson ¹, David
7 Perrais ⁵, Sandrine Fraboulet ^{1,9}, Fabien Lanté ¹, Frank Kirchhoff ³, Fiona J. Hemming ¹, Rémy
8 Sadoul ^{1,6f}

- 9
10
11 1) Grenoble Institut Neurosciences, University Grenoble Alpes- INSERM U1216- CEA, Grenoble, France
12 2) Department of Cell Biology, University of Geneva, Geneva, Switzerland.
13 3) Molecular Physiology, Center for Integrative Physiology and Molecular Medicine (CIPMM), University of
14 Saarland, Homburg, Germany.
15 4) Department of Biochemistry and Molecular Biology, Faculty of Science and Technology, University of
16 the Basque Country (UPV/EHU), Leioa, Spain.
17 5) Interdisciplinary Institute for Neuroscience, University of Bordeaux-CNRS UMR 5297, Bordeaux, France
18 6) Institut de Biologie Structurale, University Grenoble Alpes- CNRS-CEA UMR 5075, Grenoble, France
19 7) Department of Biochemistry, University of Geneva, Geneva, Switzerland.
20 8) Département des Neurosciences, Centre de Recherche du centre hospitalier de Montréal, Canada
21 9) Institute for Advanced Biosciences, Univ. Grenoble Alpes - INSERM U1209 - CNRS UMR 5309, Grenoble,
22 France

23
24
25 *Equal contribution
26 ^fCorresponding author
27 email: remy.sadoul@univ-grenoble-alpes.fr

28 **Running title:** Alix and ADBE

29
30 Number of pages: 44
31 Items number: 8 figures, 1 table, 2 movies.
32 Words count: abstract (178), introduction (655), discussion (1364).

33 Acknowledgements

34 We thank J. Brocard for helping with data analysis, Y. Saoudi for helping with fluorescence
35 microscopy, Nicolas Liaudet from the Bioimaging core facility of the University of Geneva for
36 his help with the segmentation and the electron microscopy, F. Saudou for making the MEA
37 experiments possible. We also thank K. Sadoul for critically reading the manuscript. This work
38 was funded by France Alzheimer (R.S.), Ministère de l'Enseignement Supérieur et de la
39 Recherche (K.I.C, M.R. and M.H.L.), Marie Skłodowska-Curie post-doctoral fellowship (M.M.);
40 EC H2020 MSCA-ITN EU-GliapHD #722053 (L.C.C. and F.K.), Agence Nationale de la Recherche
41 ANR (J.M.-H.) and Fondation pour la Recherche Medical FRM (E.M.).

42 Competing interests

43
44 On behalf of all authors R.Sadoul declares no competing interests.

45
46

47 **Abstract**

48 In chemical synapses undergoing high frequency stimulation, vesicle components can be
49 retrieved from the plasma membrane via a clathrin-independent process called activity
50 dependent bulk endocytosis (ADBE). Alix (ALG-2 interacting protein X)/ PDCD6IP is an adaptor
51 protein binding to ESCRT and endophilin-A proteins and thereby driving deformation and
52 fission of endosomal and cell surface membranes. In fibroblasts, Alix is required for clathrin-
53 independent endocytosis. Here, using electron microscopy, we show that synapses from mice
54 lacking Alix have subtle defects in presynaptic compartments, translating into flawed synaptic
55 plasticity. Using cultured neurons, we demonstrate that Alix is required for ADBE. We further
56 demonstrate that in order to perform ADBE, Alix must be recruited to synapses by the calcium-
57 binding protein ALG-2 and interact with endophilin-A. Finally, we show that mutant mice
58 lacking Alix in the forebrain undergo less seizures during kainate-induced status epilepticus.
59 Furthermore, propagation of the epileptiform activity to the contralateral side of kainate
60 injection is reduced. These results thus highlight Alix ko mice as an invaluable model to study
61 the exact role of ADBE at synapses undergoing physiological or pathological stimulations.

62

63 **Keywords:** PDCD6IP, Clathrin-independent-endocytosis, Alix knock-out, endophilin-A, ALG-2,
64 bulk endocytosis, synaptic vesicle recycling, synaptic transmission, calcium, epileptic
65 seizures.

66

67

68 **List of abbreviations:**

69

70 4AP: 4-Aminopyridine

71 ADBE: Activity-Dependent Bulk Endocytosis

72 ALG-2: Apoptosis Linked Gene 2

73 Alix: ALG-2 Interacting protein X

74 BAPTA: 1,2-Bis(o-AminoPhenoxy)ethane-N,N,N',N'-Tetraacetic Acid

75 BE: Bulk Endosome

76 CA1: Cornu Ammonis 1

77 CA3: Cornu Ammonis 3

78 CHMP4B: Charged Multivesicular body Protein 4B

79 CGN: Cerebellar Granule Neuron

80 CIE: Clathrin-Independent Endocytosis

81 CME: Clathrin-Mediated Endocytosis

82 CTxB: Cholera Toxin chain B

83 DIV: Day *In Vitro*

84 EGTA: Ethylene Glycol-bis(β -aminoethyl ether)-N,N,N',N'-Tetraacetic Acid

85 EM: Electron Microscope (Microscopic/ Microscopy)

86 ESCRT: Endosomal Sorting Complexes Required for Transport

87 GABA_A: γ -AminoButyric Acid type-A

88 GFP: Green Fluorescent Protein

89 HRP: Horse Radish Peroxidase

90 kDa: kiloDalton

91 KO: KnockOut

92 LTP: Long-Term Potentiation

93 N-BAR: N-terminal amphipathic helix- Bin-Amphiphysin-Rvs

94 PRD: Proline-Rich Domain

95 PSD95: Post-Synaptic Density Protein 95

96 ROI: Region of interest

97 SH3: Src Homology 3

98 SV: Synaptic Vesicle

99 Syp-pH: Synaptophysin-pHluorin

100 TSG-101: Tumour Susceptibility Gene-101

101 WT: Wild Type

102 YFP: Yellow Fluorescent Protein

103 **Introduction**

104
105 Neuronal communication in mammalian brain relies heavily on the activity-dependent
106 release of chemical neurotransmitters from presynaptic boutons. Following fusion of synaptic
107 vesicles (SV) with the presynaptic membrane, SV lipids and proteins are retrieved by
108 endocytosis. Endocytosis avoids detrimental increase in the plasma membrane surface and
109 allows recycling of the SV components to replenish the SV pool (Gan and Watanabe, 2018). At
110 moderate levels of stimulation, retrieval of membrane involves clathrin-mediated (CME) and
111 clathrin-independent endocytosis (CIE), in proportions which are still highly debated
112 (Chanaday and Kavalali, 2018). Moreover, long-lasting high-frequency stimulations also lead
113 to the clathrin-independent internalization of large stretches of pre-synaptic membranes. This
114 calcium-dependent process, first discovered at the amphibian neuromuscular junction (Miller
115 and Heuser, 1984) is referred to as activity-dependent bulk endocytosis (ADBE). It is meant to
116 avoid abnormal increase of the synaptic bouton surface and to allow replenishment of SVs
117 during sustained synaptic stimulations (Cheung and Cousin, 2012; Marxen et al., 1999). Thus,
118 ADBE has been suggested to play key regulatory roles in physiological or pathological events
119 like epilepsy, which are triggered and sustained by high frequency neuronal activity. However,
120 decrypting the physiological role of ADBE has been hindered by the lack of identified
121 molecules that are both specific and essential to this endocytosis mode.

122 We have recently demonstrated that ALG-2 interacting protein-X (Alix) is essential for
123 clathrin-independent bulk endocytosis in fibroblasts (Mercier et al., 2016). In the adult brain,
124 Alix is ubiquitously expressed but concentrates at hippocampal pre-synaptic terminals during
125 epileptic seizures (Hemming et al., 2004). Alix is a cytosolic protein first identified through its
126 calcium-dependent binding to the penta-EF-hand protein ALG-2 (apoptosis-linked gene
127 2)(Chatellard-Causse et al., 2002; Missotten et al., 1999; Sadoul, 2006). Since then, it was
128 reported that following plasma membrane wounds, ALG-2 binds to inflowing calcium and
129 helps recruiting Alix to the membrane where the latter organizes repair (Scheffer et al., 2014).
130 Alix interacts with several membrane modifying proteins among which endophilin-A proteins
131 (A1, A2 and A3) (Chatellard-Causse et al., 2002). These cytoplasmic proteins that contain an
132 N-BAR (Bin/Amphiphysin/Rvs) domain capable of sensing and generating membrane
133 curvature (Kjaerulff et al., 2011), are major actors of CME at synapses (Gad et al., 2000;
134 Ringstad et al., 1999). They also drive CIE in fibroblasts (Boucrot et al., 2014; Renard et al.,

135 2014) and were shown to control the fast mode of CIE at ribbon synapses (Llobet et al., 2011)
136 as well as in hippocampal neurons (Kononenko et al., 2014; Watanabe et al., 2018).

137 The role of Alix in bulk endocytosis in fibroblasts, its capacity to interact with endophilin-A
138 and to be recruited by calcium at membranes, together with its increased concentration at
139 hippocampal synapses during kainate-induced seizures, brought us to test its possible function
140 in ADBE. For this we made use of Alix ko mice which have normally organized but smaller
141 brains (Campos et al., 2016; Laporte et al., 2017), a phenotype that we previously linked with
142 an alteration of CIE in developing neurons (Laporte et al., 2017).

143 We now report that synapse morphology and function are both altered in Alix ko brains.
144 One obvious feature is their reduced number of synaptic vesicles and increase in size
145 correlating with impairments in synaptic facilitation and recovery during high frequency
146 stimulation. Using cultured wt neurons, we bring evidence that sustained synaptic activity
147 leads to calcium-dependent recruitment of ALG-2. ALG-2 in turn interacts with Alix, which
148 binds and concentrates endophilin-A. This protein complex is indispensable for ADBE, which
149 is selectively impaired in Alix ko neurons. Finally, we show that the number of seizures during
150 status epilepticus induced by intracortical kainate injections is reduced in conditional ko mice
151 deleted from *alix* in cortical and hippocampal neurons. In addition, the propagation of
152 epileptiform activity to the contralateral side of injection is reduced. Thus, our results show
153 that some molecular mechanisms involved in ADBE may also be involved in certain aspects of
154 synaptic plasticity such as facilitation and accommodation to synaptic fatigue and recurrence
155 of epileptic seizures.

156 **Material and methods**

157

158 Plasmids

159 Endophilin A2-mCherry was obtained by subcloning (In-Fusion Cloning kit, Clontech)
160 endophilin A2 cDNA into a pmCherry-N1 vector (Clontech). GFP-ALG-2 was obtained by
161 performing a reverse mutagenesis (Quick change II site directed mutagenesis kit, Stratagene)
162 on a GFP-hALG2 Y180A (a generous gift from Masatoshi Maki) to acquire GFP-hALG2wt. hALG2
163 E47A-E114A cDNA was kindly provided by Masatoshi Maki (Shibata et al., 2004) and was
164 subcloned into a pEGFP-C1 vector (Clontech) to obtain GFP-hALG2 E47A-E114A (GFP-
165 ALG2 Δ Ca).

166 All constructs containing Alix cDNA (wt or mutants) were obtained by subcloning the relevant
167 cDNAs from pCI vectors harbouring Alix cDNA or its mutants. Alix I212D (Alix Δ CHMP4B) and
168 Alix Δ PGY (Alix Δ ALG2) cDNAs in pCI were generated by mutagenesis (Quick change II site
169 directed mutagenesis kit, Stratagene) and Alix R757E (Alix Δ endo) by in-fusion cloning, using
170 the oligos given below.

171 mCherry-2Xflag-mAlix wt (mCherry-Alix) was obtained by subcloning 2xflag-mAlix wt cDNA
172 into a pmCherry-C1 vector (Clontech). Alix-YFP was obtained by subcloning wild type Alix cDNA
173 into a pEYFP-N1 vector (Clontech). GFP-flag-Alix (GFP-Alix) was described in (Mercier et al.,
174 2016). GFP-Alix and its mutant forms (GFP-Alix R757E, GFP-Alix Δ PGY) were obtained by
175 subcloning the various cDNAs into a pEGFP-C1 vector (Clontech). DNA constructs used for the
176 rescue experiments were prepared in two steps. First, IRES2-GFP cDNA was subcloned into
177 pSIN lentiviral vector (kindly provided by F. Saudou) by using pIRES2-GFP (Clontech) as a
178 template. Then the various cDNAs were subcloned into pSIN-IRES2-GFP.

179 Oligos used to generate mutants:

180 Alix I212D

181 sense: 5'-AAGATGAAAG ATGCCGACAT AGCTAAGCTG-3'

182 antisense: 5'-CAGCTTAGCT ATGTCGGCAT CTTTCATCTT -3'

183 Alix R757E

184 sense: 5'-CAGCCGAGCC TCCACCTCCT GTGCTTCCTG -3'

185 antisense: 5'-GAGGCTCGGC TGGAGGCTGG GGCTTAGCAG-3'

186 Alix Δ PGY

187 sense: 5'-GCCACAGGCT CAGGGATGCC AAATGCCCAT GC-3'

188 antisense: 5'-GCATGGGCAT TTGGCATCCC TGAGCCTGTG GC -3'.

189 Antibodies

190

Antibody	Supplier (reference)	Species (type)	Dilution
Anti-Actin	Millipore (MAB1501R)	Mouse (monoclonal)	1/10000
Anti-Alix	Covalab (ab0204)	Rabbit (polyclonal)	1/10000
Anti-phospho-p44/42 MAPK (T202/Y204)	Cell signaling (9106)	Mouse (monoclonal)	1/1000
Anti-PSD95	NeuroMab (73-028)	Mouse (monoclonal)	1/2000
Anti-PSD95	Millipore (MAB1598)	Mouse (monoclonal)	1/500
Anti-Synapsin-1	Millipore (AB1543P)	Rabbit (polyclonal)	1/1000
Anti-Synaptophysin	Merck Millipore (MAB5258)	Mouse (monoclonal)	1/5000
Anti-Flag	Sigma-Aldrich (F3165)	Mouse (monoclonal)	1/1000
Anti-Flag	Sigma-Aldrich (F7425)	Rabbit (polyclonal)	1/1000
Anti-Mouse HRP	Jackson ImmunoResearch (115-035-166)	Goat (polyclonal)	1/5000
Anti-Rabbit HRP	Jackson ImmunoResearch (115-035-044)	Goat (polyclonal)	1/5000
Anti-Mouse Alexa Fluor 488	Invitrogen (A-11029)	Goat (polyclonal)	1/1000
Anti-Mouse Alexa Fluor 594	Invitrogen (A-11032)	Goat (polyclonal)	1/1000
Anti-Mouse Cy5	Jackson ImmunoResearch (115-175-146)	Goat (polyclonal)	1/500
Anti-Rabbit Alexa Fluor 488	Invitrogen (A-11034)	Goat (polyclonal)	1/1000
Anti-Rabbit Alexa Fluor 594	Invitrogen (A-11037)	Goat (polyclonal)	1/1000
Anti-Rabbit Cy5	Jackson ImmunoResearch (111-175-144)	Goat (polyclonal)	1/1000

191

192 Animals

193 Animals were handled and killed in conformity with European law and internal regulations of
194 INSERM. Pregnant Oncins France souche A (OFA; a substrain of Sprague Dawley) rats (Charles
195 River) were used for rat neuronal cultures. Alix ko C57BL/6 mouse pups (Laporte et al., 2017;

196 Mercier et al., 2016) and their control littermates referred to thereafter as Alix wt, were also
197 used for primary neuronal culture. Transgenic mice were held at the animal facility of the
198 Grenoble Institute for Neurosciences and fed *ad libitum*. All animals were held at a twelve-
199 hour light/dark cycle. One to two month-old Alix wt and Alix ko mice were used for
200 electrophysiological recordings, histochemistry and electron microscopy studies.

201 Mice were anesthetized by intraperitoneal injection of 0.1 ml sodium pentobarbital (5.6% w/v;
202 CEVA Santé Animale) and treated as described in the corresponding sub-headings of the
203 material and methods section.

204 $Emx1^{IREScre}/Alix^{fl/fl}$ and $Emx1^{IREScre}$ control mice were used for the kainate injection epilepsy
205 model. 8-11 weeks old mice were anesthetized under a mixture of 2 % isoflurane, 47.5 % O₂
206 and 47.5 % N₂O. Transgenic mice were held at the animal facility of the CIPMM and fed *ad*
207 *libitum*. All animals were held at a twelve-hour light/dark cycle. This study was carried out in
208 strict accordance with the European and German guidelines for the welfare of experimental
209 animals. Animal experiments were approved by the Saarland state's "Landesamt für
210 Gesundheit und Verbraucherschutz" animal licence number 36/2016.

211

212 Golgi staining

213 2-month-old anesthetized mice were dislocated prior to brain dissection and 100 µm thick
214 coronal brain sections were cut on a vibratome in the hippocampal region. The dendritic
215 spines of hippocampal neurons from the CA1 *stratum radiatum* were visualized by the Golgi
216 impregnation technique. For this, we used the FD Rapid GolgiStain kit (FD NeuroTechnologies).
217 Brain sections were immersed in equal volumes of solutions A and B for 7 d and impregnated
218 with solution C for 48 h at 4°C. Then, the sections were washed twice in double-distilled water
219 and incubated for 10 min in a mixture of one part of solution D, one part of solution E, and
220 two parts of double-distilled water. Sections were washed twice, dehydrated with increasing
221 concentrations of ethanol, and mounted with epoxy resin (Fluka) between two coverslips.
222 Stacks of bright-field images with 0.3 µm spacing were acquired with a Zeiss Axioskop 50
223 microscope with 63x oil objective (NA 1.4; Plan-Apochromat) coupled to a CCD camera
224 (CoolSnap ES; Roper Scientific) operated by Metaview software (Molecular Devices). Images
225 were analysed with ImageJ. The number of dendritic spines (>1 µm protrusion of 100 µm
226 portions of dendrite) per unit dendritic length was counted with ImageJ.

227

228 Transmission electron microscopy of the CA1 hippocampus

229 2-month-old, anesthetized mice were intracardially perfused with phosphate-buffered 0.9%
230 NaCl (PBS), followed by 0.1 M phosphate buffered 4% paraformaldehyde, pH 7.4,
231 supplemented with 0.05% glutaraldehyde (Sigma). The brains were carefully removed,
232 postfixed for 4 h in the same fixative and 60 μm sections were cut with a vibratome. After
233 several washes in PBS, the sections were postfixed in 1% glutaraldehyde in the same buffer
234 for 10 min and processed for EM. This included treatment with osmium tetroxide (1% in 0.1
235 M PB), block staining with uranyl acetate, dehydration through a graded series of ethanol, and
236 flat embedding on glass slides in Durcupan (Fluka) resin. Regions of interest were cut at 70 nm
237 on an ultramicrotome (Reichert Ultracut E; Leica) and collected on one-slot copper grids.
238 Staining was performed on drops of 1% aqueous uranyl acetate, followed by Reynolds's lead
239 citrate. EM images were acquired in a JEOL-1200 electron microscope with a digital camera
240 (Veleta, SIS; Olympus) and analysed with ImageJ. Twenty images per animal from 3 animals
241 per genotype were used for quantification. The number of synapses per μm^2 was calculated.
242 A synapse was considered if it met 3 criteria: a presynaptic bouton filled with at least 10
243 synaptic vesicles (1) juxtaposed to the head of a dendritic spine with a clearly visible PSD (2)
244 and the presence of the neck in the section (3). Number of synaptic vesicles and areas of
245 presynaptic boutons were quantified in each synapse using the free-shape tool and the cell
246 counter plugins of ImageJ. We used the straight tool of ImageJ to measure the lengths of PSDs,
247 and head and neck diameters. Note that the head diameter was taken parallel to the PSD and
248 the neck diameter was perpendicular to the neck membranes.

249

250 Electrophysiological recordings in CA1

251 *Ex vivo slice preparation:* Brain slices were prepared from 2-month-old C57BL/6 wt and Alix ko
252 mice. The brains were removed quickly and 350 μm -thick sagittal slices containing both cortex
253 and hippocampus were cut in ice-cold sucrose solution (2.5 mM KCl, 1.25 mM NaH_2PO_4 , 10
254 mM MgSO_4 , 0.5 mM CaCl_2 , 26 mM NaHCO_3 , 234 mM sucrose, 11 mM glucose, saturated with
255 95% O_2 and 5% CO_2) with a Leica VT1200 blade microtome (Leica Microsystems, Nanterre,
256 France). After cutting, hippocampi were extracted from the slice and transferred to
257 oxygenated Artificial Cerebro-Spinal Fluid (ACSF: 119 mM NaCl, 2.5 mM KCl, 1.25 mM NaH_2PO_4 ,
258 1.3 mM MgSO_4 , 2.5 mM CaCl_2 , 26 mM NaHCO_3 , 11 mM glucose) at $37 \pm 1^\circ\text{C}$ for 30 min and
259 then kept at room temperature for at least 1 h before recordings. Each slice was individually

260 transferred to a submersion-type recording chamber and continuously superfused (2 ml/min)
261 with oxygenated ACSF. Extracellular recordings were obtained at 28°C from the apical
262 dendritic layers of the hippocampal CA1 area, using glass micropipettes filled with ACSF. Field
263 excitatory postsynaptic potentials (fEPSPs) were evoked by the electrical stimulation of
264 Schaffer collaterals afferent to CA1. The magnitude of the fEPSPs was determined by
265 measuring their slope. Signals were acquired using a double EPC 10 Amplifier (HEKA Elektronik
266 Dr. Schulze GmbH, Germany) and analysed with Patchmaster software (HEKA Elektronik Dr.
267 Schulze GmbH, Germany).

268 *Input/output*: The slope of fEPSPs was plotted as a function of stimulation intensity (30 to 60
269 μ A).

270 *Paired-pulse facilitation (PPF)*: PPF of synaptic transmission was induced by paired-pulse
271 stimulation with an inter-stimulus interval of 50 ms. PPF was quantified by normalising the
272 second response to the first one.

273 *Frequency facilitation*: Schaffer collaterals were stimulated repetitively by 25 stimuli of the
274 same intensity at 25Hz.

275 *Long-term potentiation*: Test stimuli were delivered once every 15 s. Stimulus intensities were
276 adjusted to produce 40-50% of the maximal response. A stable baseline was recorded for at
277 least 15 min. LTP was induced by high frequency stimulation (4 trains delivered at 100 Hz with
278 5 min between each train). Average value of fEPSP slope was expressed as a percentage of the
279 baseline response.

280

281 EEG telemetry and unilateral intracortical kainate injection

282 We took advantage of the unilateral intracortical kainate injection model for human temporal
283 lobe epilepsy. Telemetric EEG transmitter implantation, kainate injection and data analysis
284 was adapted from Bedner and colleagues (Bedner et al., 2015).

285 Alix^{fl/fl} mice (Laporte et al., 2017) with heterozygous cre expression (Emx1^{IREScree} (Emx^{tm1(cre)Krlj},
286 MGI: 2684610)(Gorski et al., 2002)) as well as control mice (Alix^{fl/fl} x Emx^{wt}) were implanted
287 with telemetric EEG transmitters (DSI PhysioTel® ETA-F10, Harvard Biosciences, Inc. Holliston,
288 Massachusetts, USA) between 8 and 11 weeks of age. The animals were placed in a stereotaxic
289 frame (Robot stereotaxic, Neurostar, Tübingen, Germany) for implantation of depth
290 electrodes at 3.4 mm posterior to bregma and bilaterally 1.6 mm from the sagittal suture.
291 After post-surgical care and recovery, mice were again placed in the stereotaxic frame and

292 injected with 70 nl of a 20 mM solution of kainate (Tocris, Wiesbaden-Nordenstadt, Germany)
293 in 0.9% NaCl, above the right dorsal hippocampus (1.9 mm posterior to bregma, 1.5 mm from
294 sagittal suture and 1.3 mm from skull surface). Kainate was injected at a rate of 70 nl/ min
295 with a 10 µl Nanofil syringe (34 GA blunt needle, World Precision Instruments, Sarasota, FL,
296 USA). The syringe was kept in place for 2 min after the injection was completed to avoid liquid
297 reflux.

298 Cages were placed on individual radio receiving plates (DSI PhysioTel® RPC-1, Data Sciences
299 International, St. Paul, USA), which record EEG signals and sent them, together with the video
300 recording (MediaRecorder Software, Noldus Information Technology, Wageningen,
301 Netherlands), to an input exchange matrix (DSI PhysioTel® Matrix 2.0 (MX2), Ponemah
302 software, DSI, Data Sciences International, St. Paul, USA). The animals were monitored for at
303 least 20 h post kainate injection. In our model the mortality rate associated to *status*
304 *epilepticus* is less than 5% in more than 50 mice with different genetic backgrounds over the
305 last 12 months.

306 **Immunohistochemistry**

307 Free-floating vibratome sections (40 µm) were incubated for one hour in blocking buffer
308 (5 % HS, 0.3 % Triton X in 1x PBS) at room temperature. Sections were incubated with
309 primary antibodies (rabbit@Iba1 [1:500], Wako; goat@GFAP [1:1000], Abcam) diluted in
310 blocking solution, overnight at 4°C. Secondary antibodies (Alexa546@rabbit [1:1000];
311 Alexa488@goat [1:1000], Invitrogen) and DAPI (0.025 µg/ml, Sigma) were diluted in blocking
312 buffer and incubated for 2 h at room temperature.

313 *Data analysis:* EEG traces were analysed with the Neuroscore software (Version 3.3.1., Data
314 Sciences International, St. Paul, USA). Electrographic seizures were detected with the spike
315 detection protocol. Subsequently, an additional manual screen was employed to remove
316 artifacts that were eventually picked up. Seizures were characterized by high frequency
317 spiking and ceased with a postictal depression (flattening of EEG). Seizure detection was
318 complemented by synchronized video monitoring. Electrographic seizures were associated
319 with behavioural analogues of Racine stages II-V (Racine, 1972). The total duration of *status*
320 *epilepticus* was defined from the first electrographic seizure to the first seizure free period
321 lasting 1 h. Statistical analysis was performed with GraphPad Prism.

322

323 Cell culture and transfection

324 Cortical and hippocampal neurons from rat E18 embryos and P0 Alix wt and ko mice were
325 prepared as previously described (Faure et al., 2006). Briefly, cortices and hippocampi were
326 dissected from E18 rat embryos or P0 mouse pups, treated with trypsin, and mechanically
327 dissociated. Dissociated cells were seeded at a density of $5 \times 10^4/\text{cm}^2$ in 100 mm dishes for
328 cortical neurons and $1.5 \times 10^4/\text{cm}^2$ onto acid-washed coverslips (either 14 mm diameter or 25
329 mm; Marienfeld) in either 4-well plates or P35 dishes (ThermoScientific) precoated for 4 h
330 with 50 $\mu\text{g}/\text{ml}$ poly-D-lysine (Sigma). Neurons were maintained in neuronal culture medium
331 (Neurobasal medium containing 2% B27 supplement, 10 unit/mL penicillin, 10 $\mu\text{g}/\text{mL}$
332 streptomycin, and 0.5 mM L-glutamine; Invitrogen) supplemented with 10% heat-inactivated
333 horse serum (Invitrogen). Neurons were maintained in water-saturated 95% air/5% CO_2 at
334 37°C. The seeding medium was replaced after 20 h with serum-free neuronal culture medium.

335 Neurons were transfected at 10 DIV as previously described (Chassefeyre et al., 2015). Briefly,
336 for each P35 dish, 2 μg plasmid DNA, 250 mM CaCl_2 were mixed with an equal volume of 2x
337 BES-buffered saline and left to precipitate for 20 min at room temperature. Neurons were
338 placed in transfection medium (Minimum Essential Medium containing 0.22% NaHCO_3 , 20 mM
339 D-glucose and 0.5 mM L-glutamine) supplemented with 2% B27, before the DNA precipitate
340 was added. They were then incubated for 1.5 h at 37°C and 5% CO_2 . Neurons were then
341 washed by being placed in transfection medium (pre-warmed to 37°C in 10% CO_2) for 20 min
342 at 37°C and 5% CO_2 . Finally, they were transferred back into their conditioned medium.

343 Primary cultures of cerebellar granule neurons (CGN) were prepared from 6-day-old C57BL/6
344 Alix wt and Alix ko pups as described previously (Trioulier et al., 2004), with some

345 modifications. The cerebella were removed, cleared of their meninges, and cut into 1-mm
346 pieces. They were then incubated at 37°C for 10 min in 0.25% trypsin-EDTA and DNase (1500
347 U/mL). Trypsin was inactivated and cells were dissociated in culture medium (DMEM
348 containing 10% fetal bovine serum, 2 mM L-glutamine, 25 mM KCl, 10 mM HEPES and 10
349 unit/ml penicillin, 10 µg/ml streptomycin). After filtration on 70 µm cell strainers, neurons
350 were plated at $5 \cdot 10^5$ cell/cm² onto poly-D-lysine (10 µg/ml, Sigma) precoated coverslips.
351 Cytosine-β-D-arabinoside (10 µM, Sigma) was added after 1 day in vitro (DIV), to prevent the
352 growth of non-neuronal cells, until 8 DIV when neurons were used for activity dependent bulk
353 endocytosis experiment (see below).

354

355 Multi-electrode array

356 Dissociated hippocampal neurons were resuspended in neuronal medium and plated at a 10⁶
357 cells/cm² on poly-L-lysine-coated multi-electrode arrays comprising 59 extracellular recording
358 electrodes and one reference electrode (MEA-60 Multichannel Systems, MCS). Electrodes
359 were 30 µm in diameter and separated by a distance of 200 µm. MEA-60 plates were
360 connected to a 60-channel data acquisition system (USB-MEA64) and associated amplifier
361 (MEA1060-Inv-BC) powered by a PS40W power supply system (MCS, Germany). The recording
362 system was then placed in a humidified incubation chamber at 37°C and 5% CO₂. Neurons
363 were left for 5 min to equilibrate before recording. Basal spontaneous activity was recorded
364 for 3 min prior addition of drugs. Bicuculline (100 µM) and 4-aminopyridine (5 mM) were then
365 added and neuronal activity recorded for another 10 min. Signals were recorded with a 1100
366 gain, sampled at 20 kHz and analyzed with MC Rack software (MCS, Germany). Raw signals
367 were first filtered with a Butterworth band pass filter (2nd order) between 200 and 800 Hz to
368 remove electrical noise and low frequency signals. Spike detection analysis was performed on
369 filtered signals using a threshold of 6 standard deviations to mark out action potentials. Burst
370 events were identified as a minimum of 5 consecutive spikes with an interspike interval lower
371 than 100 ms. The minimum interval time between two bursts was fixed at 1000 ms.
372 Representative traces were exported using custom-made Matlab functions (Matlab 2014b).

373

374 Imaging of synaptophysin-pHluorin upon electrical stimulation

375 Hippocampal neurons from Alix wt and ko mice were transfected with synaptophysin-pHluorin
376 (Syp-pH) at 6 DIV by a calcium phosphate transfection procedure. The recycling of synaptic

377 vesicles was imaged in a buffer solution containing 120 mM NaCl, 5 mM KCl, 2 mM CaCl₂, 2
378 mM MgCl₂, 5 mM glucose, 10 mM HEPES adjusted to pH 7.4 and 270 mOsm/l. Experiments
379 were carried out at 34°C. Neurons were stimulated by electric field stimulation (platinum
380 electrodes, 10 mm spacing, 1 ms pulses of 50 mA and alternating polarity at 5-40 Hz) applied
381 by a constant current stimulus isolator (SIU-102, Warner Instruments). The presence of 10 μM
382 6-cyano-7-nitroquinoxaline-2,3-dione (CNQX) and 50 μM D,L-2-amino-5-phosphonovaleric
383 acid (AP5) prevented recurrent activity.

384 Experiments were performed on an inverted microscope (IX83, Olympus) equipped with an
385 Aplanachromat N oil 100× objective (NA 1.49). Images were acquired with an electron multiplying
386 charge coupled device camera (QuantEM:512SC; Roper Scientific) controlled by MetaVue7.1
387 (Roper Scientific). Samples were illuminated by a 473-nm laser (Cobolt). Emitted fluorescence
388 was detected after passing a 525/50 nm filter (Chroma Technology Corp.). Time-lapse images
389 were acquired at 1 or 2 Hz with integration times from 50 to 100 ms.

390 Image analysis was performed with custom macros in Igor Pro (Wavemetrics) using an
391 automated detection algorithm as described previously (Martineau et al., 2017). The image
392 from the time series showing maximum response during stimulation was subjected to an “à
393 trous” wavelet transformation. All identified masks and calculated time courses were visually
394 inspected for correspondence to individual functional boutons. The intensity values were
395 normalized to the ten frames before stimulation.

396

397 Live Fluorescence Imaging of Alix and endophilin recruitment to synapses

398 For live imaging of protein recruitment, cultured hippocampal neurons were co-transfected
399 with Alix-mCherry or endophilin-A2-mCherry together with Syp-pH expression vectors 2 to 4
400 days prior to imaging. All live imaging experiments were performed at 37°C and images were
401 acquired using a spinning disk confocal microscope (AxioObserver Z1) with a 63x oil objective
402 (NA 1.46, Zeiss) at 488 nm and 561 nm excitation. Transfected neurons were placed in basal
403 medium for 10 min and then mounted in an imaging chamber (POC-R2 Cell cultivation system,
404 Zeiss). Imaging lasted 12 min and consisted of 2 min in basal medium, 5 min in bicuculline/4AP
405 solution and 5 min in basal medium. A 5x bicuculline/4AP solution was added (final
406 concentration, 100 μM and 5 mM, respectively) for stimulation which lasted 5 min and the
407 chamber was perfused with basal medium at 3 ml/min for washing. ROI were drawn on
408 ‘presynapses’ defined by spots of synaptophysin-pHluorin that increased during stimulation.

409 For both synaptophysin-pHluorin and mCherry-Alix, fluorescence values were measured in
410 these ROI and then normalised to the initial fluorescence values (fluorescence values prior to
411 stimulation) using ImageJ.

412

413 Immunofluorescence

414 Cultured hippocampal neurons were fixed for 20 min at room temperature in phosphate-
415 buffered 4% paraformaldehyde supplemented with 4% sucrose. After three washes in PBS,
416 cells were permeabilized and blocked in PBS containing 0.3% Triton X-100 and 3% BSA for 15
417 min at room temperature. Coverslips were incubated for 1–2 h at room temperature with
418 primary antibodies diluted in the blocking solution. After washing in PBS, cells were incubated
419 for 1 h with secondary antibodies conjugated to Alexa Fluor 488, Alexa Fluor 594, or Cyanine
420 5 (Cy5), diluted in the blocking solution. Coverslips were rinsed and mounted in Mowiol.
421 Images were acquired on a Leica SPE microscope using a 40x dry objective (NA 0.75, Leica) or
422 a 100x oil immersion objective (NA 1.4, Leica) at 488 nm, 532 nm or 635 nm.

423 *Synapse density*: Cultured hippocampal neurons were fixed and stained with antibodies at 14-
424 16 DIV as described above. Presynaptic boutons (synapsin-1-positive) and postsynaptic
425 terminals (PSD95-positive) were selected using the Spot Detector plugin in Icy software
426 (de Chaumont et al., 2012) (wavelet detection with size filtering between 0.4 μm and 2 μm in
427 diameter) on max image projections. Synapses were defined as spots of colocalization
428 between the detected presynaptic and postsynaptic terminals that were within 3 μm of each
429 other. Synapses were counted using the Colocalization Studio in ICY software (Lagache et al.,
430 2018)

431 *Protein recruitment assays*: Cultured hippocampal neurons were transfected with expression
432 vectors 24~48 h prior to stimulation. The transfected neurons were incubated in basal
433 medium (150 mM NaCl, 5 mM KCl, 1.3 mM CaCl_2 , 10 mM HEPES and 33 mM D-glucose at pH
434 7.4) for 10 min prior to stimulation. Coverslips were either treated with basal medium alone
435 or bicuculline/4AP solution (basal medium supplemented with 100 μM bicuculline and 5 mM
436 4-aminopyridine) for 5 min at 37°C and 5% CO_2 . Coverslips were fixed and stained with
437 antibodies against synapsin-1 and PSD95 as described above. Images were acquired on a Leica
438 SPE microscope using a 100x oil immersion objective (NA 1.4, Leica) at 488 nm, 532 nm or 635
439 nm. The acquired images were analysed using ImageJ. Regions of interest (ROI) were drawn
440 on areas of axons which colocalize with anti-synapsin-1 spots, but not with anti-PSD95 spots

441 to ensure presynaptic measurement. Fluorescence intensities were then measured in these
442 ROI and normalised to fluorescence intensities measured on other regions of axons to give the
443 relative fluorescence intensity at presynaptic boutons.

444

445 Quantification of calcium increase during stimulation

446 Hippocampal neurons cultured on 24-well plates were placed in basal medium and incubated
447 with 1 μ M Fluo-4-AM for 1 h at 37°C. After washing, neurons were left in 250 μ l basal medium
448 for 5 min. Plates were then transferred to a Pherastar automatic plate reader (BMG Labtech,
449 Germany) set to 37 °C, to record fluorescence intensity at 0.1 Hz during 590 s, for each well,
450 and with fluorescence measurement settings as described on
451 <http://www.bmglabtech.com/media/35216/1043854.pdf>. Neurons were stimulated with 50
452 μ l 6x bicuculline/4AP solution (final concentration, 100 μ M and 5 mM, respectively) after 290
453 s with automatic injection.

454

455 Quantification of ADBE by dextran uptake

456 The protocol for dextran uptake was adapted from (Clayton and Cousin, 2009b). 15-17 DIV
457 hippocampal neurons were stimulated with bicuculline/4AP solution for 5 min, at 37°C and 5%
458 CO₂, in the presence of 10 kDa tetramethylrhodamine-dextran (50 μ M). Coverslips were
459 immediately washed several times in washing solution (basal medium supplemented with 0.2%
460 BSA and warmed to 37°C) to remove excess dextran. For ADBE inhibition, neurons were
461 stimulated in the presence of 2 μ M GSK3 inhibitor (CT99021, Tocris) and placed in fresh basal
462 medium containing 2 μ M GSK3 inhibitor for 10 min at 37°C and 5% CO₂. Neurons were then
463 fixed as previously described and imaged with a Leica SPE microscope using a 40x dry
464 immersion objective (NA 0.75, Leica) at 532 nm excitation. Analysis was performed on ImageJ.
465 The number of fluorescent spots was counted in a defined field of view (130 μ m x 130 μ m) in
466 thresholding analysis with a diameter limit between 300 nm and 2 μ m (resolution limit for the
467 microscope and maximum size of a nerve terminal).

468 *Rescue experiments:* Cultured hippocampal neurons were transfected 2 to 4 d prior to the day
469 of experiment. Dextran uptake assay was performed as described above. Images were
470 acquired on a Leica SPE microscope using a 40x oil immersion objective (NA 1.25, Leica) at 488
471 nm and 532 nm excitation. The analysis was performed on ICY software. ROI were generated
472 closely around axons by using 'thresholder'. Then dextran spots within these ROI were

473 counted by using 'spot detector' with size limit between 300 nm and 2 μ m. The length of axon
474 per field of view was estimated by manually drawing 'Polyline type ROI' over the axon images.
475 The number of dextran spots per μ m of axon was calculated and expressed as ratio to control
476 values.

477

478 EM examination of ADBE in culture neurons

479 Analysis of ADBE from cerebellar granule neurons was performed as described previously with
480 some modifications (Cheung et al., 2010). 8 DIV CGN were pre-incubated in hyperpolarizing
481 medium (170 mM NaCl, 3.5 mM KCl, 0.4 mM KH₂PO₄, 20 mM TES, 5 mM NaHCO₃, 5 mM D-
482 glucose, 1.2 mM Na₂SO₄, 1.2 mM MgCl₂, 1.3 mM CaCl₂, pH7.4) for 10 min prior to stimulation.
483 Neurons were then incubated for 2 min with 10 mg/ml HRP (Sigma P8250) in either the
484 hyperpolarizing medium or a high-potassic solution containing 50 mM KCl (123.5 mM NaCl, 50
485 mM KCl, 0.4 mM KH₂PO₄, 20 mM TES, 5 mM NaHCO₃, 5 mM D-glucose, 1.2 mM Na₂SO₄, 1.2
486 mM MgCl₂, 1.3 mM CaCl₂, pH7.4) before rapid washing in PBS and fixation in PBS-
487 glutaraldehyde 2% for 30 min. After three washes in Tris buffer 100 mM, endocytosed HRP
488 was revealed by incubation in Tris 100 mM containing 0.1% diaminobenzidine and 0.2% H₂O₂.
489 The cultures were then post-fixed in 1% osmium tetroxide, dehydrated and embedded in Epon.
490 Synapses were photographed with a JEOL-1200 electron microscope. Quantification was
491 performed as follows: HRP-positive structures were quantified per synapse and classified as
492 synaptic vesicles when the diameter was less than 100 nm and as bulk endosome when the
493 diameter was more than 100 nm.

494 For focused ion beam scanning electron microscopy (FIB-SEM), the block was mounted on a
495 pin, coated with gold, and inserted into the chamber of a HELIOS 660 Nanolab DualBeam
496 SEM/FIB microscope (FEI Co., Eindhoven, The Netherlands). Region of interest (ROI) was
497 prepared using focused ion beam (FIB) and ROI set to be approximately 15 μ m wide. During
498 the acquisition process, the image acquisition parameters of the electron beam were 2 kV and
499 0.4 nA and the thickness of the FIB slice between each image acquisition was 10 nm. The
500 segmentation of the synapse and ADBE was done with Amira software (Thermo Fisher
501 Scientist) and the movie obtained using Imaris (Oxford Instruments).

502

503 Synaptosomal preparation from cortical neurons

504 Synaptosome-enriched membranes from 15 DIV cortical neurons were prepared as described

505 previously with some modifications (Frandemiche et al., 2014). Briefly, cultured neurons were
506 stimulated for 15 min with a mixture of bicuculline/4AP (50 μ M/2.5 mM). After a wash in HBSS,
507 neurons were homogenized by passing 15-20 times through 0.25G needle in cold buffer
508 containing 0.32 M sucrose, 10 mM HEPES, 15mM NaF, 15mM β -glycerophosphate and
509 protease inhibitors (Roche), pH 7.4. Samples were maintained at 4°C during all steps of the
510 experiment. Homogenates were cleared at 1000g for 10 min to remove nuclei and large debris.
511 The resulting supernatants were spun down at 12,000 g for 20 min to obtain a crude
512 membrane fraction and washed twice in HEPES buffer 4 mM containing 1 mM EDTA, 15 mM
513 NaF, 15 mM β -glycerophosphate and protease inhibitors (Roche), pH 7.4. The resulting pellet
514 was solubilized in 0.5% Triton X-100, 20 mM HEPES, 100 mM NaCl, 15mM NaF, 15 mM β -
515 glycerophosphate, pH 7.2, containing protease inhibitors (Roche) for 20 min at 4°C with mild
516 agitation and analysed by Western blot.

517

518 Western blot

519 Cells lysates were resuspended in Laemmli buffer and resolved by SDS-PAGE in 10%
520 polyacrylamide gels. Proteins were electro-transferred onto PVDF membranes that were then
521 blocked for 30 min in TBS containing 0.1% Tween 20 and 5% dry milk and incubated for 1 h to
522 overnight with primary antibodies diluted in the blocking solution. After washes in TBS–Tween,
523 the membranes were further incubated for 1 h with secondary antibodies coupled to HRP,
524 washed as before and incubated with luminescence-generating HRP substrate. Bound
525 antibodies were revealed by luminography on film.

526

527 Statistical analysis

528 The comparison of two groups was performed using Student's t-test or its non-parametric
529 correspondent, the Mann-Whitney test, if normality was not granted either because not
530 checked or because rejected (Shapiro-Wilks test). The comparisons of more than two groups
531 were made using one or two way ANOVAs followed by post-hoc tests (Holm Sidak's or Tukey's
532 HSD, see table 1 for details) to identify all the significant group differences. N indicates
533 independent biological replicates. The graphs with error bars indicate 1 SEM (+/-) except for
534 figure 1C-H where we used box plots showing distribution of medians (whiskers = min and
535 max values). The significance level is denoted as usual (* p <0.05, ** p <0.01, *** p <0.001). All
536 the statistical analyses were performed using Prism7 (Graphpad version 7.0a, April 2, 2016).

537 Means, confidence intervals, degrees of freedom and p values were calculated using Prism7.

538 Effect sizes are either those reported by the software or Cohen's D calculated as the difference

539 of means divided by the pooled weighted standard deviation:

540
$$(|m_1 - m_2|) / \sqrt{\left(SD_1^2 \times \frac{n_1}{(n_1+n_2)} \right) + \left(SD_2^2 \times \frac{n_2}{(n_1+n_2)} \right)}.$$

541 The results of the statistical analyses are listed in table 1.

542

543 Results

544 Alix is required for synaptic plasticity

545 To study the effect of Alix on the number of synapses, we first compared brains of Alix ko
546 (Laporte et al., 2017) and wt mice and found that the density of dendritic spines in the CA1
547 hippocampal region of adult brains stained with Golgi-Cox was not different (Supplementary
548 figure 1). Similarly, EM examination of the same CA1 hippocampal region revealed no
549 difference in the number of synaptic contacts between wt and Alix ko neurons (Figure 1A). In
550 cultured hippocampal neurons, the number of synapses revealed by co-immunostaining with
551 synapsin-1 and PSD95, was similar between wt and Alix ko (Figure 1B) indicating that Alix is
552 not required for synaptogenesis. However, EM of the CA1 *stratum radiatum* of adult mice
553 showed that Alix ko synapses contained significantly fewer synaptic vesicles (SV) than wt
554 (Figure 1C, D). Furthermore, the size of postsynaptic densities, known to be strictly correlated
555 with the number of SV (Harris and Stevens, 1989), was similarly reduced in Alix ko synapses
556 (Figure 1F, G). Importantly, the surface of Alix ko synaptic boutons was also significantly
557 increased suggesting plasma membrane accumulation in these synapses (Figure 1C, E). Finally,
558 at the postsynaptic level, we also noticed that the ratio between the diameter of the spine
559 head and that of the neck was changed in Alix ko animals suggesting possible defects in
560 maturation or plasticity of adult synapses lacking Alix (Figure 1F, H).

561 Using electrophysiological recordings of acute hippocampal slices from adult animals, we
562 next examined if the morphological differences detected in Alix ko synapses might translate
563 into alterations of their function. For this, we performed field recordings in the CA1 *stratum*
564 *radiatum* of hippocampal slices during stimulation of Schaffer collaterals. As shown on figure
565 2A the input-output curves were not significantly different between Alix ko and wt animals
566 indicating that, in this region, both the connectivity and the basal synaptic transmission are
567 not grossly affected by the lack of Alix. However, in the same slices, long-term potentiation
568 (LTP) induced by tetanic stimulations was significantly impaired in Alix ko, compared to wt
569 hippocampal slices (average recordings between 25 and 35 min post-high-frequency
570 stimulation: 105.02 ± 13.86 % in Alix ko compared to 180.70 ± 11.19 % in wt, Figure 2B). In the
571 same CA3/CA1 synapses, the paired-pulse facilitation ratio was significantly reduced in ko
572 animals (1.43 ± 0.04 in ko vs 1.62 ± 0.07 in wt, Figure 2C). Furthermore, synaptic fatigue,
573 induced by repeated stimulations at 25 Hz, was significantly increased in absence of Alix

574 (Figure 2D). Thus, electrophysiological recordings reveal presynaptic anomalies, which may be
575 related to impairments in high frequency-induced LTP.

576

577 Alix is recruited to synapses upon synaptic activation.

578 We next used dissociated cortical neuron cultures to decipher the role of Alix at synapses.
579 Western blot analysis during *in vitro* differentiation revealed that Alix expression strongly
580 increases during synaptogenesis as indicated by the parallel rise in postsynaptic density
581 protein 95 (PSD95) expression (Figure 3A). Moreover, synaptosome-enriched membranes
582 prepared from cortical neurons (15 DIV) contained Alix (Figure 3B). This synaptic pool
583 increased when neuron cultures were incubated 15 min with the GABA_A receptor antagonist
584 bicuculline, together with a weak potassium channel blocker 4-aminopyridine (4AP)(Figure 3B),
585 a treatment known to increase the frequency of action potential bursts and thereby induce
586 sustained intracellular calcium elevation (Supplementary figure 2A) (Hardingham et al., 2001;
587 Hardingham et al., 2002). Therefore, this observation suggests that Alix tends to concentrate
588 at synapses undergoing prolonged stimulations. To show that this is indeed the case, we used
589 live imaging to follow mCherry-Alix relocation to synapses in 15 DIV hippocampal neurons.
590 While the fluorescent signal was homogeneously distributed throughout the entire neuronal
591 cytoplasm in resting conditions (Figure 3C, t= 0 min), it almost doubled in discrete spots within
592 neuronal processes during synaptic activation corresponding to active presynaptic boutons
593 labelled with Synaptophysin-pHluorin (Syp-pH) (Granseth et al., 2006) (arrowheads Figure 3C,
594 t= 2:20, 4 and 6 min; Movie 1). Alix recruitment to these sites is concomitant with the
595 activation of glutamatergic synapses, as it became detectable a few seconds after addition of
596 bicuculline/4AP to the culture medium and decreased soon after washing the cells (Figure 3
597 C, D). Thus, we demonstrate that mCherry-Alix recruitment occurs at presynaptic sites that
598 display transient increase of Syp-pH fluorescence induced by stimulation (arrowheads Figure
599 3C, Figure 3D; Movie 1). Alix localization at axonal boutons was confirmed in bicuculline/4AP
600 stimulated and fixed-neurons expressing Alix-YFP and immunolabelled for synapsin-1 to reveal
601 presynaptic boutons (Figure 3E, F). Similar experiments using anti-PSD95 immunostaining
602 showed that Alix-positive spots were juxtaposed to but did not overlap with the postsynaptic
603 density marker (Figure 3G). Measuring Alix-YFP fluorescence intensities in dendritic spines
604 before and during stimulation showed no accumulation of Alix at the post-synaptic level

605 (Supplementary figure 2B, C), further demonstrating that synaptic activation leads to Alix
606 recruitment only at pre-synaptic parts.

607

608 Recruitment of Alix partners, ALG-2 and endophilin-A, at activated synapses

609 In non-neuronal cells, Alix recruitment to plasma membrane wounds was shown to be
610 caused by calcium entry. Calcium binds ALG-2, a penta-EF-hand containing protein, which
611 thereafter interacts with Alix allowing its recruitment to the plasma membrane (Scheffer et
612 al., 2014). In neurons, action potential depolarization induces massive and transient calcium
613 accumulation in the bouton, which triggers fusion of SV with the plasma membrane. Adding
614 the intra-cellular calcium chelators BAPTA-AM or EGTA-AM completely abolished Alix-YFP
615 recruitment (Supplementary figure 3). Interestingly, GFP-ALG-2 concentrated at presynaptic
616 boutons upon synaptic activation (Figure 4A, B), in contrast to an ALG-2 point-mutant unable
617 to bind calcium (ALG-2 Δ Ca) (Figure 4B). ALG-2 recruitment does not depend on Alix, as it
618 concentrates at stimulated synapses of both wt and Alix ko neurons (Figure 4B, 4C left bars).
619 On the contrary, Alix recruitment to active synapses is tightly dependent on its capacity to
620 interact with ALG-2, as a mutated version of the protein unable to interact with ALG-2
621 (Alix Δ ALG-2) (Suzuki et al., 2008; Trioulier et al., 2004) does not accumulate at presynaptic
622 boutons upon stimulation (Figure 4C, right bars).

623 Among other partners of Alix, endophilins-A are main regulators of endocytosis at synapses
624 and impact the number of SVs (Milosevic et al., 2011; Schuske et al., 2003). We therefore
625 tested if endophilins could be recruited to active synapses, similarly to Alix and ALG-2.
626 Endophilin-A2-mCherry was mainly detected at presynaptic boutons but its fluorescence
627 increased during bicuculline/4AP treatment (Figure 4D, E; Movie 2). Remarkably, no such
628 increase could be seen in Alix ko neurons, whereas Alix deleted of its endophilin binding
629 domain (Alix Δ endo), was still able to be recruited to synapses upon activation (Figure 4F). This
630 observation strongly suggests that the increase in endophilin concentration during sustained
631 synaptic activation requires Alix expression.

632

633 Alix is required for ADBE

634 Altogether, our observations indicate that calcium increase at synapses undergoing
635 sustained activity allows the transient recruitment of ALG-2/Alix and endophilin-A to pre-
636 synaptic parts. Because of our EM observations showing that Alix ko axonal bouton are bigger

637 and have significantly fewer SVs, we next tested which step of the turnover of presynaptic
638 vesicles might be affected by the lack of the protein. We used Syp-pH expressing neurons and
639 followed their fluorescence during electrical stimulation to trigger exocytosis. Recapture of
640 synaptic proteins from the plasma membrane results in decay in fluorescence, reflecting SV
641 retrieval and vesicle re-acidification (Soykan et al., 2017). As illustrated in figures 5A and B,
642 fluorescence increases during stimulation (exocytosis) followed by a decrease thereafter
643 (endocytosis), with no drastic difference between Alix ko and wt neurons for the two
644 stimulation frequencies, 5 and 40 Hz. However, the time constant of the exponential decay
645 was slightly decreased in Alix ko neurons stimulated at 40 Hz, suggesting a higher rate of Syp-
646 pH endocytosis occurring at this frequency (Figure 5B).

647 We next tested if the protein might intervene in activity-dependent bulk endocytosis
648 (ADBE) at synapses. Cultured cerebellar granular neurons (CGN) have been extensively used
649 to study this process (Cheung et al., 2010). Here, neurons were depolarized with 50 mM KCl,
650 in the presence of Horse Radish Peroxidase (HRP) that is endocytosed and fills vesicles and
651 endosomes as they form. EM examination of wt synapses showed that depolarization
652 dramatically increased the number of vacuoles decorated by HRP. We verified using FIB SEM
653 and 3D reconstruction that these vacuoles had undergone fission from the plasma membrane
654 and could therefore be identified as bulk endosomes (Figure 5C yellow arrowheads; Figure
655 5D). Other HRP positive vesicles having the size of neurotransmitter vesicles were also more
656 numerous in depolarized synapses (Figure 5C blue arrowheads; Figure 5D, E). In Alix ko
657 synapses, the number of depolarization-induced bulk endosomes was strongly reduced
658 (Figure 5E, F). Consistent with the increased endocytic rate detected by Syp-pH in Alix ko
659 neurons stimulated at 40 Hz (Figure 5B), the number of newly formed SV was significantly
660 increased, suggesting a mechanism compensating for ADBE deficiency (Figure 5G).

661 Another way to assess for ADBE is by the use of fluorescent 10 kDa dextran, a fluid phase
662 cargo that accumulates inside bulk endosomes but fails to label vesicles formed by clathrin-
663 dependent mechanisms upon neuronal stimulation (Clayton and Cousin, 2009a). Hippocampal
664 neurons incorporated dextran when incubated in presence of bicuculline/4AP. A GSK3
665 inhibitor, known to block ADBE but not other modes of SV endocytosis (Clayton et al., 2010),
666 completely abolished the dextran labelling (Supplementary figure 4A, B). In contrast, Alix ko
667 neurons failed to endocytose dextran (Figure 6A, B) even though bicuculline/4AP stimulation
668 increased calcium entry (Supplementary figure 2A) and neuronal activity (Supplementary

669 figure 4C, D) in both Alix ko and wt neurons. As already shown (Morton et al., 2015), neurons
670 also failed to endocytose dextran when treated with calcium chelators BAPTA and EGTA
671 (Supplementary figure 4E), both of which blocked Alix recruitment to presynaptic boutons
672 (Supplementary figure 3). Finally, rescue experiments showed that the impairment in ADBE
673 observed in Alix ko cells is due solely to the absence of Alix, since restoring Alix expression
674 fully restored the capacity of Alix ko cells to endocytose 10 kDa dextran (Figure 6 C, D). In sharp
675 contrast, expression of Alix Δ ALG-2 or Alix Δ Endo was not able to rescue dextran endocytosis
676 by Alix ko neurons (Figure 6I). Noteworthy, an Alix mutant (Alix Δ 4B) unable to bind the ESCRT-
677 III protein CHMP4B, was still able to rescue ADBE in Alix ko neuron. These results demonstrate
678 that the capacity of Alix to drive ADBE requires interaction with both endophilin-A and ALG-2
679 but not with ESCRT-III.

680

681 Alix conditional-ko mice undergo less kainate induced acute seizures.

682 The physiological relevance of ADBE remains today unclear but it is thought that it allows
683 synapses to sustain high frequency stimulations such as those seen during epilepsy. We tested
684 this possibility by studying the acute phase of a mouse model for human temporal lobe
685 epilepsy (Bedner et al., 2015). The unilateral intracortical kainate injection induces the acute
686 phase, *status epilepticus*, characterized by high seizure frequency, during several hours.
687 Seizure activity was determined by telemetric EEG recording and synchronized video
688 monitoring (Figure 7A, B). Here we used Alix conditional-ko mice where Alix is deleted in
689 neocortical and hippocampal excitatory neurons (Gorski et al., 2002) (Figure 7A). The total
690 duration of *status epilepticus* (SE) was comparable in Alix ko (median 1.70 h; Interquartile
691 range, IQR = 1.85) and control mice (1.63 h; IQR = 2.55, Figure 7C). However, Alix ko mice
692 experienced about 66 % less seizures than control mice (8; IQR = 13 seizures in ko vs. 18;
693 IQR = 23 in control, Figure 7D). The average seizure duration was only minimally reduced in
694 Alix ko compared to control (25.7 s; IQR = 19.36 vs. 32.9 s; IQR = 19.54, Figure 7E). These
695 results show that the absence of Alix selectively reduces the number of high frequency events
696 (single seizures), without affecting the total duration of *status epilepticus*.

697 The intracortical kainate injection model of temporal lobe epilepsy employed here produces
698 seizures originating from the hippocampus, which can secondarily generalize and thereby
699 spread to other (contralateral) brain areas. After EEG recording, 24 h post kainate injection,
700 the brains were processed for immunohistochemical analysis (Figure 8) to assess microglial

701 (Iba1) reactivity in cortex (Figure 8A, B, D) and hippocampus (Figure 8A, C, D). In both control
702 and Alix ko animals, quantification of Iba1 fluorescence intensity revealed an enhanced
703 microglia activation on the ipsilateral side, related to the kainate injection (Figure 8B, C, E).
704 While the difference between ipsi-and contralateral side was non-significant in control
705 animals ($\approx 10\%$), Alix ko animals displayed a significantly reduced contralateral microglial
706 activation ($\approx 30\%$, $p=0.009$) (Figure 8E). As expected, this difference between Alix ko and wt
707 animals was not seen using GFAP immunolabelling, reflecting the fact that astroglial activation
708 peaks only 4-7 days after a CNS insult. (Supplementary figure 5). The reduced contralateral
709 microglial activation seen in Alix ko animals is an indicator for reduced propagation of the
710 seizure activity, corroborating the previous seizure quantification (Figure 7D).

711 In summary, Alix is specifically required for ADBE. Impairment in this process seen in Alix
712 ko mice could be related to the lower number of SV and increase in the surface of presynaptic
713 membranes observed *in vivo*, as well as to impairments in synaptic function and plasticity in
714 normal and pathological settings.

715

716 Discussion

717 To sustain neurotransmission and prevent expansion of the presynaptic plasma membrane,
718 synaptic vesicle (SV) fusion is coupled to the endocytic recycling and regeneration of SV
719 proteins and lipids. Vesicle components can be retrieved from the plasma membrane via
720 clathrin scaffolds, or via clathrin-independent processes mediating fast and ultrafast
721 endocytosis and, in the case of high frequency stimulation, bulk endocytosis (Gan and
722 Watanabe, 2018). Using Alix ko cells, we recently discovered that Alix drives clathrin-
723 independent-endocytosis (CIE) during ligand-induced endophilin-dependent endocytosis as
724 well as bulk endocytosis (Laporte et al., 2017; Mercier et al., 2016). Furthermore, we had
725 previously reported that Alix immunoreactivity in the rat hippocampus is strongly upregulated
726 in synapses undergoing high frequency activation during kainate-induced epileptic seizures.
727 Interestingly, endophilin-A and synaptophysin stainings revealed that this increase was
728 presynaptic and only transient, as it was reversed soon after cessation of the seizures
729 (Hemming et al., 2004). In order to study the possible role of Alix recruitment to presynaptic
730 parts seen during seizures, we used primary cultures of cortical and hippocampal neurons
731 which make networks undergoing spontaneous activities. Adding 4-aminopyridine (4-AP), a
732 weak potassium channel blocker, together with bicuculline to block GABA_A receptors, greatly
733 increases spike frequency (Sup. Figure 6 C, D) and results in elevated calcium entry (sup. Figure
734 3A)(Hardingham et al., 2001). Consistent with the kainate-induced Alix increase seen during
735 epileptic seizures, bicuculline/4AP induced Alix to transiently concentrate at presynaptic parts
736 of firing synapses. The use of dextran uptake to monitor bulk endocytosis revealed that the
737 very same treatment triggered activity dependent bulk endocytosis (ADBE) which required
738 Alix expression. Despite this, monitoring the decay of Syp-pH fluorescence did not reveal any
739 obvious blockage of the endocytosis of the protein at 40 Hz. This is in good agreement with
740 observations showing that at these frequencies, Syp-pH reveals synaptic CME or CIE but not
741 ADBE (Nicholson-Fish et al., 2015; Soykan et al., 2017). In fact, Syp-pH fluorescent decay in Alix
742 ko hippocampal neurons suggested an increase in endocytosis, confirmed by EM in cerebellar
743 neurons, which could represent a compensatory process for the absence of Alix and
744 concomitant ADBE impairment. Thus, the use of Alix ko neurons revealed that Alix is required
745 for ADBE at synapses but does not seem to be involved in SV endocytosis.

746 ADBE is triggered by high [Ca²⁺] in response to sustained activity (Paillart et al., 2003).
747 Calcium and calmodulin-dependent phosphatase calcineurin were suggested to make a link

748 between synaptic activity and formation of bulk endosomes through dynamin (Morton et al.,
749 2015). Alix may represent another link as its recruitment and activity in ADBE seems
750 dependent on calcium increase. EGTA, which binds calcium at an approximately 100 times
751 slower on-rate than BAPTA (Adler et al., 1991; Schneggenburger and Neher, 2005), and was
752 already known to block ADBE without affecting synaptic release, was equally efficient as
753 BAPTA in inhibiting Alix recruitment. This recruitment required Alix capacity to bind the
754 calcium-binding protein ALG-2, which also concentrated at hyperactive synapses. ALG-2 is a
755 cytosolic penta-EF hand-containing protein with two Ca^{2+} binding sites ($K_d = 1.2 \mu\text{M}$), and its
756 interaction with Alix strictly depends on calcium (Missotten et al., 1999; Shibata et al., 2004;
757 Trioulier et al., 2004). Conformational change and exposure of hydrophobic patches occur at
758 μM concentrations of Ca^{2+} , suggesting that ALG-2 functions as a calcium sensor (Maki et al.,
759 2016). Indeed, in non-neuronal cells, calcium entry provoked by membrane wounds leads to
760 the sequential recruitment to the membrane of ALG-2, Alix and ESCRT-III proteins necessary
761 for membrane repair (Jimenez et al., 2014; Scheffer et al., 2014). In neurons, the activity-
762 dependent accumulation of ALG-2 at synapses required Ca^{2+} binding as it was totally abolished
763 by point-mutations within the two Ca^{2+} binding sites. Interestingly, ALG-2 recruitment at
764 synapses did not require Alix, as it also occurred in Alix ko neuron. Thus, our observations
765 highlight synaptic ALG-2 as an obvious candidate for sensing calcium elevation and suggest
766 the following scenario: sustained high frequency depolarization leads to massive elevation of
767 calcium in the synaptic bouton; Ca^{2+} binding to ALG-2 causes its accumulation at the synaptic
768 membrane and binding to cytosolic Alix, whose recruitment to the membrane drives ADBE. It
769 remains unclear how ALG-2 interacts with lipid bilayers (Maki et al., 2016; Scheffer et al., 2014).
770 For Alix, a change in conformation induced by binding to ALG-2 allows its interaction with
771 lysobisphosphatidic acid (LBPA), a phospholipid only present in late endosomes (Bissig and
772 Gruenberg, 2014; Bissig et al., 2013; Sun et al., 2015). If they exist, equivalent lipids from the
773 plasma membrane favouring Alix recruitment remain to be discovered.

774 Little is known about the molecular mechanisms underlying the plasma membrane
775 deformation during ADBE. The proline rich domain of Alix interacts with the SH3 domains of
776 endophilins-A1-3 which contain N-BAR domains and have been shown to regulate clathrin-
777 dependent and -independent SV endocytosis at different synapses (Gad et al., 2000; Llobet et
778 al., 2011; Ringstad et al., 1999). BAR domains are dimerization domains able to induce,
779 stabilize and sense membrane curvature (Farsad et al., 2001; Kjaerulff et al., 2011).

780 Interestingly, a proteomic approach has recently revealed the presence of endophilin-A1, Alix
781 and ALG-2 in bulk endosomes (Kokotos et al., 2018). Furthermore, endophilin-A2, actin and
782 dynamin mediate a restricted type of CIE activated upon ligand binding to cargo receptors
783 (Boucrot et al., 2014; Renard et al., 2014). Endophilin-A and Alix act in the same CIE pathway,
784 even if Alix is more promiscuous for ligands, as it is also involved in fluid phase endocytosis. In
785 fibroblasts, interaction of Alix with endophilins favours their presence at the membrane
786 (Mercier et al., 2016). In hippocampal neurons, endophilin-A2 decorated presynapses of
787 resting neurons but Alix was needed for its synaptic increase during stimulation. In turn, Alix
788 recruitment did not need interaction with endophilins to be recruited. Concave cytoplasmic
789 surfaces of the plasma membrane are thought to trigger the recruitment of endophilin-A
790 through their BAR domains (Boucrot et al., 2014; Kjaerulff et al., 2011). At synapses, Alix might
791 represent an adaptor concentrating endophilins onto the flat membranes of the peri-active
792 zone to drive membrane bending in response to high calcium concentrations. Alix-endophilin
793 complex is required for ADBE, as demonstrated by the lack of rescue of ADBE by an Alix point
794 mutant unable to interact with endophilin, a finding reminiscent of that seen in the case of
795 CIE of Cholera Toxin B (CTxB) (Mercier et al., 2016). Interestingly, the incapacity of Alix to
796 interact with Chmp4B from ESCRT-III, known to alleviate its plasma membrane repair ability
797 (Jimenez et al., 2014; Scheffer et al., 2014), did not alter rescue of ADBE. This result also
798 discriminates Alix-driven ADBE from roles of the ESCRT system in the degradation of SV
799 proteins (Sadoul et al., 2017; Sheehan et al., 2016).

800 The role of ADBE *in vivo* is not fully understood, in part due to a lack of models in which
801 synaptic ADBE is selectively impaired. The severe LTP impairment and increased synaptic
802 fatigue observed in Alix ko hippocampus could be related to the difficulty of synapses to deal
803 with the repeated stimulations necessary to trigger potentiation. As such, they represent a
804 first demonstration of the necessity of ADBE for normal synaptic plasticity. Excitatory,
805 glutamatergic neurotransmission plays a central role in the generation of seizure activity
806 (Albrecht and Zielińska, 2017; Barker-Haliski and White, 2015) and figures among the primary
807 anti-epileptic drug targets (Rogawski and Löscher, 2004). Sustained, intense and synchronous
808 neurotransmission as occurring during seizures requires replenishment of synaptic vesicle
809 pools mainly through activity-dependent bulk endocytosis (ADBE) (Cheung and Cousin, 2012).
810 Impairing ADBE *in vivo*, by deleting Alix in neocortical and hippocampal excitatory neurons
811 (Gorski et al., 2002), led to a significantly reduced number of seizures during SE, without

812 affecting the total duration of SE or the mean seizure duration. The present results suggest
813 that excitatory networks lacking Alix have a reduced capacity to initiate sequential seizures,
814 due to an impaired replenishment of synaptic vesicles through ADBE. Seizure termination and
815 *status epilepticus* cessation however seem to be governed by distinct mechanisms, probably
816 involving inhibitory transmission to re-establish the balance between excitation and inhibition
817 in the brain. Our results highlight Alix ko mice as an invaluable tool for exploring and
818 understanding more precisely the exact role of ADBE at synapses undergoing normal and
819 pathological stimulations.

820 References

- 821
- 822 Adler, E.M., G.J. Augustine, S.N. Duffy, and M.P. Charlton. 1991. Alien intracellular calcium
823 chelators attenuate neurotransmitter release at the squid giant synapse. *J Neurosci.*
824 11:1496-1507.
- 825 Albrecht, J., and M. Zielińska. 2017. Mechanisms of Excessive Extracellular Glutamate
826 Accumulation in Temporal Lobe Epilepsy. *Neurochem Res.* 42:1724-1734.
- 827 Barker-Haliski, M., and H.S. White. 2015. Glutamatergic Mechanisms Associated with
828 Seizures and Epilepsy. *Cold Spring Harb Perspect Med.* 5:a022863.
- 829 Bedner, P., A. Dupper, K. Huttmann, J. Muller, M.K. Herde, P. Dublin, T. Deshpande, J.
830 Schramm, U. Haussler, C.A. Haas, C. Henneberger, M. Theis, and C. Steinhauser.
831 2015. Astrocyte uncoupling as a cause of human temporal lobe epilepsy. *Brain.*
832 138:1208-1222.
- 833 Bissig, C., and J. Gruenberg. 2014. ALIX and the multivesicular endosome: ALIX in
834 Wonderland. *Trends Cell Biol.* 24:19-25.
- 835 Bissig, C., M. Lenoir, M.C. Velluz, I. Kufareva, R. Abagyan, M. Overduin, and J. Gruenberg.
836 2013. Viral infection controlled by a calcium-dependent lipid-binding module in ALIX.
837 *Dev Cell.* 25:364-373.
- 838 Boucrot, E., A.P. Ferreira, L. Almeida-Souza, S. Debard, Y. Vallis, G. Howard, L. Bertot, N.
839 Sauvonnet, and H.T. McMahon. 2014. Endophilin marks and controls a clathrin-
840 independent endocytic pathway. *Nature.*
- 841 Campos, Y., X. Qiu, E. Gomero, R. Wakefield, L. Horner, W. Brutkowski, Y.G. Han, D. Solecki,
842 S. Frase, A. Bongiovanni, and A. d'Azzo. 2016. Alix-mediated assembly of the
843 actomyosin-tight junction polarity complex preserves epithelial polarity and epithelial
844 barrier. *Nature communications.* 7:11876.
- 845 Chanaday, N.L., and E.T. Kavalali. 2018. Time course and temperature dependence of
846 synaptic vesicle endocytosis. *FEBS Lett.* 592:3606-3614.
- 847 Chassefeyre, R., J. Martinez-Hernandez, F. Bertaso, N. Bouquier, B. Blot, M. Laporte, S.
848 Fraboulet, Y. Coute, A. Devoy, A.M. Isaacs, K. Pernet-Gallay, R. Sadoul, L. Fagni, and Y.
849 Goldberg. 2015. Regulation of Postsynaptic Function by the Dementia-Related ESCRT-
850 III Subunit CHMP2B. *J Neurosci.* 35:3155-3173.
- 851 Chatellard-Causse, C., B. Blot, N. Cristina, S. Torch, M. Missotten, and R. Sadoul. 2002. Alix
852 (ALG-2-interacting protein X), a protein involved in apoptosis, binds to endophilins
853 and induces cytoplasmic vacuolization. *J Biol Chem.* 277:29108-29115.
- 854 Cheung, G., and M.A. Cousin. 2012. Adaptor protein complexes 1 and 3 are essential for
855 generation of synaptic vesicles from activity-dependent bulk endosomes. *J Neurosci.*
856 32:6014-6023.
- 857 Cheung, G., O.J. Jupp, and M.A. Cousin. 2010. Activity-dependent bulk endocytosis and
858 clathrin-dependent endocytosis replenish specific synaptic vesicle pools in central
859 nerve terminals. *J Neurosci.* 30:8151-8161.
- 860 Clayton, E.L., and M.A. Cousin. 2009a. The molecular physiology of activity-dependent bulk
861 endocytosis of synaptic vesicles. *J Neurochem.* 111:901-914.
- 862 Clayton, E.L., and M.A. Cousin. 2009b. Quantitative monitoring of activity-dependent bulk
863 endocytosis of synaptic vesicle membrane by fluorescent dextran imaging. *J Neurosci*
864 *Methods.* 185:76-81.
- 865 Clayton, E.L., N. Sue, K.J. Smillie, T. O'Leary, N. Bache, G. Cheung, A.R. Cole, D.J. Wyllie, C.
866 Sutherland, P.J. Robinson, and M.A. Cousin. 2010. Dynamin I phosphorylation by

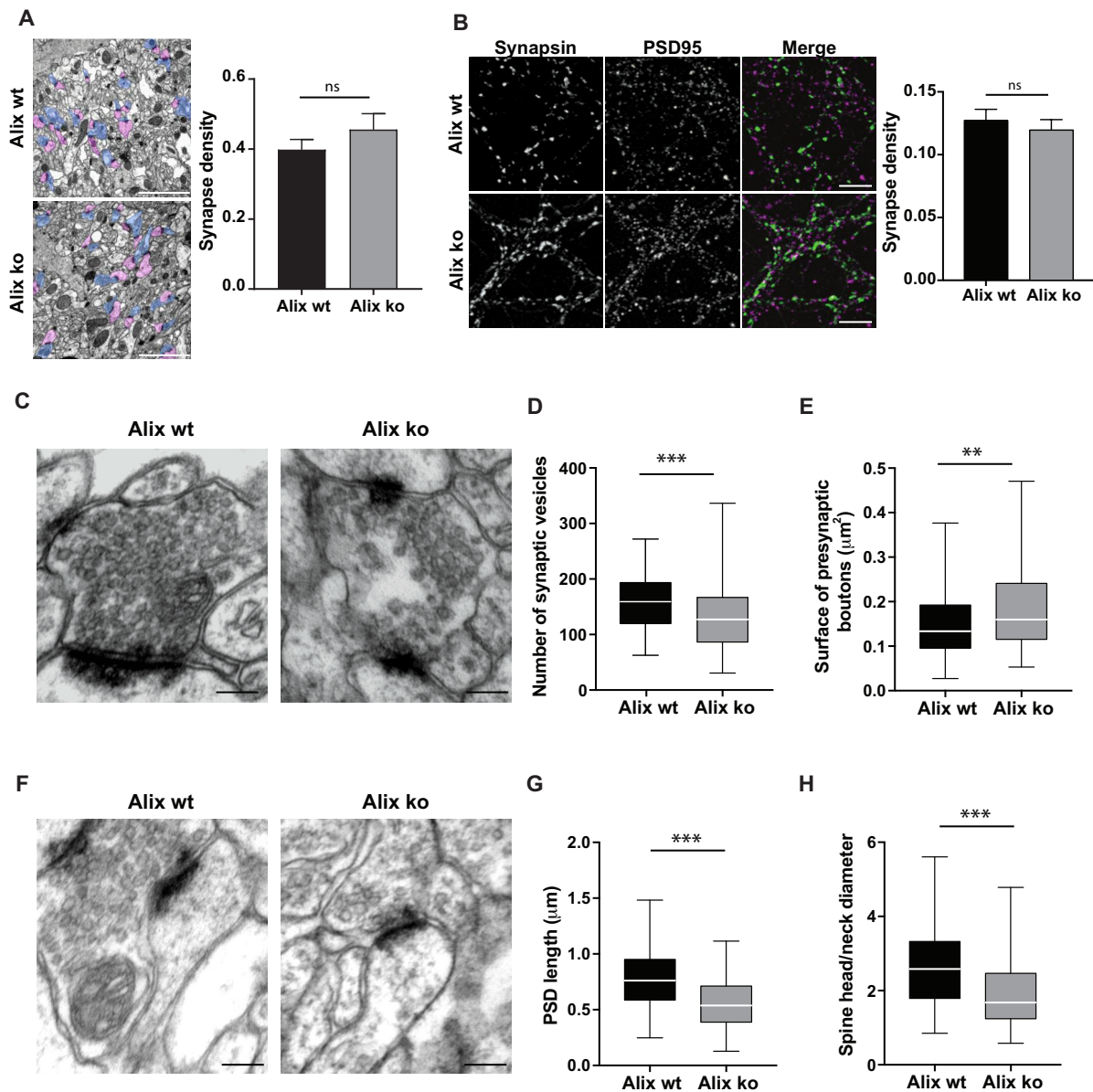
- 867 GSK3 controls activity-dependent bulk endocytosis of synaptic vesicles. *Nat Neurosci.*
868 13:845-851.
- 869 de Chaumont, F., S. Dallongeville, N. Chenouard, N. Herve, S. Pop, T. Provoost, V. Meas-
870 Yedid, P. Pankajakshan, T. Lecomte, Y. Le Montagner, T. Lagache, A. Dufour, and J.C.
871 Olivo-Marin. 2012. Icy: an open bioimage informatics platform for extended
872 reproducible research. *Nature methods.* 9:690-696.
- 873 Farsad, K., N. Ringstad, K. Takei, S.R. Floyd, K. Rose, and P. De Camilli. 2001. Generation of
874 high curvature membranes mediated by direct endophilin bilayer interactions. *J Cell*
875 *Biol.* 155:193-200.
- 876 Faure, J., G. Lachenal, M. Court, J. Hirrlinger, C. Chatellard-Causse, B. Blot, J. Grange, G.
877 Schoehn, Y. Goldberg, V. Boyer, F. Kirchhoff, G. Raposo, J. Garin, and R. Sadoul. 2006.
878 Exosomes are released by cultured cortical neurones. *Mol Cell Neurosci.* 31:642-648.
- 879 Frandemiche, M.L., S. De Seranno, T. Rush, E. Borel, A. Elie, I. Arnal, F. Lante, and A. Buisson.
880 2014. Activity-dependent tau protein translocation to excitatory synapse is disrupted
881 by exposure to amyloid-beta oligomers. *J Neurosci.* 34:6084-6097.
- 882 Gad, H., N. Ringstad, P. Low, O. Kjaerulff, J. Gustafsson, M. Wenk, G. Di Paolo, Y. Nemoto, J.
883 Crun, M.H. Ellisman, P. De Camilli, O. Shupliakov, and L. Brodin. 2000. Fission and
884 uncoating of synaptic clathrin-coated vesicles are perturbed by disruption of
885 interactions with the SH3 domain of endophilin. *Neuron.* 27:301-312.
- 886 Gan, Q., and S. Watanabe. 2018. Synaptic Vesicle Endocytosis in Different Model Systems.
887 *Frontiers in cellular neuroscience.* 12:171.
- 888 Gorski, J.A., T. Talley, M. Qiu, L. Puelles, J.L. Rubenstein, and K.R. Jones. 2002. Cortical
889 excitatory neurons and glia, but not GABAergic neurons, are produced in the Emx1-
890 expressing lineage. *J Neurosci.* 22:6309-6314.
- 891 Granseth, B., B. Odermatt, S.J. Royle, and L. Lagnado. 2006. Clathrin-mediated endocytosis is
892 the dominant mechanism of vesicle retrieval at hippocampal synapses. *Neuron.*
893 51:773-786.
- 894 Hardingham, G.E., F.J. Arnold, and H. Bading. 2001. Nuclear calcium signaling controls CREB-
895 mediated gene expression triggered by synaptic activity. *Nat Neurosci.* 4:261-267.
- 896 Hardingham, G.E., Y. Fukunaga, and H. Bading. 2002. Extrasynaptic NMDARs oppose synaptic
897 NMDARs by triggering CREB shut-off and cell death pathways. *Nat Neurosci.* 5:405-
898 414.
- 899 Harris, K.M., and J.K. Stevens. 1989. Dendritic Spines of Ca-1 Pyramidal Cells in the Rat
900 Hippocampus - Serial Electron-Microscopy with Reference to Their Biophysical
901 Characteristics. *Journal of Neuroscience.* 9:2982-2997.
- 902 Hemming, F.J., S. Fraboulet, B. Blot, and R. Sadoul. 2004. Early increase of apoptosis-linked
903 gene-2 interacting protein X in areas of kainate-induced neurodegeneration.
904 *Neuroscience.* 123:887-895.
- 905 Jimenez, A.J., P. Maiuri, J. Lafaurie-Janvore, S. Divoux, M. Piel, and F. Perez. 2014. ESCRT
906 machinery is required for plasma membrane repair. *Science.* 343:1247136.
- 907 Kjaerulff, O., L. Brodin, and A. Jung. 2011. The structure and function of endophilin proteins.
908 *Cell biochemistry and biophysics.* 60:137-154.
- 909 Kokotos, A.C., J. Peltier, E.C. Davenport, M. Trost, and M.A. Cousin. 2018. Activity-dependent
910 bulk endocytosis proteome reveals a key presynaptic role for the monomeric GTPase
911 Rab11. *Proc Natl Acad Sci U S A.* 115:E10177-E10186.
- 912 Kononenko, N.L., D. Puchkov, G.A. Classen, A.M. Walter, A. Pechstein, L. Sawade, N. Kaempfer,
913 T. Trimbuch, D. Lorenz, C. Rosenmund, T. Maritzen, and V. Haucke. 2014.

- 914 Clathrin/AP-2 mediate synaptic vesicle reformation from endosome-like vacuoles but
915 are not essential for membrane retrieval at central synapses. *Neuron*. 82:981-988.
- 916 Lagache, T., A. Grassart, S. Dallongeville, O. Faklaris, N. Sauvonnnet, A. Dufour, L. Danglot, and
917 J.C. Olivo-Marin. 2018. Mapping molecular assemblies with fluorescence microscopy
918 and object-based spatial statistics. *Nature communications*. 9:698.
- 919 Laporte, M.H., C. Chatellard, V. Vauchez, F.J. Hemming, J.C. Deloulme, F. Vossier, B. Blot, S.
920 Fraboulet, and R. Sadoul. 2017. Alix is required during development for normal
921 growth of the mouse brain. *Sci Rep*. 7:44767.
- 922 Llobet, A., J.L. Gallop, J.J. Burden, G. Camdere, P. Chandra, Y. Vallis, C.R. Hopkins, L. Lagnado,
923 and H.T. McMahon. 2011. Endophilin drives the fast mode of vesicle retrieval in a
924 ribbon synapse. *J Neurosci*. 31:8512-8519.
- 925 Maki, M., T. Takahara, and H. Shibata. 2016. Multifaceted Roles of ALG-2 in Ca(2+)-Regulated
926 Membrane Trafficking. *Int J Mol Sci*. 17.
- 927 Martineau, M., A. Somasundaram, J.B. Grimm, T.D. Gruber, D. Choquet, J.W. Taraska, L.D.
928 Lavis, and D. Perrais. 2017. Semisynthetic fluorescent pH sensors for imaging
929 exocytosis and endocytosis. *Nature communications*. 8.
- 930 Marxen, M., W. Volkandt, and H. Zimmermann. 1999. Endocytic vacuoles formed following
931 a short pulse of K⁺ -stimulation contain a plethora of presynaptic membrane
932 proteins. *Neuroscience*. 94:985-996.
- 933 Mercier, V., M.H. Laporte, O. Destaing, B. Blot, C.M. Blouin, K. Pernet-Gallay, C. Chatellard, Y.
934 Saoudi, C. Albiges-Rizo, C. Lamaze, S. Fraboulet, A. Petiot, and R. Sadoul. 2016. ALG-2
935 interacting protein-X (Alix) is essential for clathrin-independent endocytosis and
936 signaling. *Sci Rep*. 6:26986.
- 937 Miller, T.M., and J.E. Heuser. 1984. Endocytosis of synaptic vesicle membrane at the frog
938 neuromuscular junction. *J Cell Biol*. 98:685-698.
- 939 Milosevic, I., S. Giovedi, X. Lou, A. Raimondi, C. Collesi, H. Shen, S. Paradise, E. O'Toole, S.
940 Ferguson, O. Cremona, and P. De Camilli. 2011. Recruitment of endophilin to clathrin-
941 coated pit necks is required for efficient vesicle uncoating after fission. *Neuron*.
942 72:587-601.
- 943 Missotten, M., A. Nichols, K. Rieger, and R. Sadoul. 1999. Alix, a novel mouse protein
944 undergoing calcium-dependent interaction with the apoptosis-linked-gene 2 (ALG-2)
945 protein. *Cell Death Differ*. 6:124-129.
- 946 Morton, A., J.R. Marland, and M.A. Cousin. 2015. Synaptic vesicle exocytosis and increased
947 cytosolic calcium are both necessary but not sufficient for activity-dependent bulk
948 endocytosis. *J Neurochem*. 134:405-415.
- 949 Nicholson-Fish, J.C., A.C. Kokotos, T.H. Gillingwater, K.J. Smillie, and M.A. Cousin. 2015.
950 VAMP4 Is an Essential Cargo Molecule for Activity-Dependent Bulk Endocytosis.
951 *Neuron*. 88:973-984.
- 952 Paillart, C., J. Li, G. Matthews, and P. Sterling. 2003. Endocytosis and vesicle recycling at a
953 ribbon synapse. *J Neurosci*. 23:4092-4099.
- 954 Racine, R.J. 1972. Modification of seizure activity by electrical stimulation. II. Motor seizure.
955 *Electroencephalogr Clin Neurophysiol*. 32:281-294.
- 956 Renard, H., M. Simunovic, J. Lemiere, E. Boucrot, M.D. Garcia-Castillo, S. Arumugam, V.
957 Chambon, C. Lamaze, C. Wunder, A.K. Kenworthy, A.A. Schmidt, H.T. McMahon, C.
958 Sykes, P. Bassereau, and L. Johannes. 2014. Endophilin-A2 functions in membrane
959 scission in clathrin-independent endocytosis. *Nature*.

- 960 Ringstad, N., H. Gad, P. Low, G. Di Paolo, L. Brodin, O. Shupliakov, and P. De Camilli. 1999.
961 Endophilin/SH3p4 is required for the transition from early to late stages in clathrin-
962 mediated synaptic vesicle endocytosis. *Neuron*. 24:143-154.
- 963 Rogawski, M.A., and W. Löscher. 2004. The neurobiology of antiepileptic drugs. *Nat Rev*
964 *Neurosci*. 5:553-564.
- 965 Sadoul, R. 2006. Do Alix and ALG-2 really control endosomes for better or for worse. *Bio*.
966 *Cell*. 98:69-77.
- 967 Sadoul, R., M.H. Laporte, R. Chassefeyre, K.I. Chi, Y. Goldberg, C. Chatellard, F.J. Hemming,
968 and S. Fraboulet. 2017. The role of ESCRT during development and functioning of the
969 nervous system. *Semin Cell Dev Biol*.
- 970 Scheffer, L.L., S.C. Sreetama, N. Sharma, S. Medikayala, K.J. Brown, A. Defour, and J.K.
971 Jaiswal. 2014. Mechanism of Ca(2+)-triggered ESCRT assembly and regulation of cell
972 membrane repair. *Nature communications*. 5:5646.
- 973 Schneggenburger, R., and E. Neher. 2005. Presynaptic calcium and control of vesicle fusion.
974 *Curr Opin Neurobiol*. 15:266-274.
- 975 Schuske, K.R., J.E. Richmond, D.S. Matthies, W.S. Davis, S. Runz, D.A. Rube, A.M. van der
976 Blik, and E.M. Jorgensen. 2003. Endophilin is required for synaptic vesicle
977 endocytosis by localizing synaptojanin. *Neuron*. 40:749-762.
- 978 Sheehan, P., M. Zhu, A. Beskow, C. Vollmer, and C.L. Waites. 2016. Activity-Dependent
979 Degradation of Synaptic Vesicle Proteins Requires Rab35 and the ESCRT Pathway. *J*
980 *Neurosci*. 36:8668-8686.
- 981 Shibata, H., K. Yamada, T. Mizuno, C. Yorikawa, H. Takahashi, H. Satoh, Y. Kitaura, and M.
982 Maki. 2004. The penta-EF-hand protein ALG-2 interacts with a region containing PxY
983 repeats in Alix/AIP1, which is required for the subcellular punctate distribution of the
984 amino-terminal truncation form of Alix/AIP1. *J Biochem (Tokyo)*. 135:117-128.
- 985 Soykan, T., N. Kaempfer, T. Sakaba, D. Vollweiter, F. Goerdeler, D. Puchkov, N.L. Kononenko,
986 and V. Haucke. 2017. Synaptic Vesicle Endocytosis Occurs on Multiple Timescales and
987 Is Mediated by Formin-Dependent Actin Assembly. *Neuron*. 93:854-866 e854.
- 988 Sun, S., X. Zhou, J. Corvera, G.E. Gallick, S.H. Lin, and J. Kuang. 2015. ALG-2 activates the MVB
989 sorting function of ALIX through relieving its intramolecular interaction. *Cell Discov*.
990 1:15018.
- 991 Suzuki, H., M. Kawasaki, T. Inuzuka, M. Okumura, T. Kakiuchi, H. Shibata, S. Wakatsuki, and
992 M. Maki. 2008. Structural basis for Ca²⁺-dependent formation of ALG-2/Alix peptide
993 complex: Ca²⁺/EF3-driven arginine switch mechanism. *Structure*. 16:1562-1573.
- 994 Trioulier, Y., S. Torch, B. Blot, N. Cristina, C. Chatellard-Cause, J.M. Verna, and R. Sadoul.
995 2004. Alix, a protein regulating endosomal trafficking, is involved in neuronal death. *J*
996 *Biol Chem*. 279:2046-2052.
- 997 Watanabe, S., L.E. Mamer, S. Raychaudhuri, D. Luvsanjav, J. Eisen, T. Trimbuch, B. Sohl-
998 Kielczynski, P. Fenske, I. Milosevic, C. Rosenmund, and E.M. Jorgensen. 2018.
999 Synaptojanin and Endophilin Mediate Neck Formation during Ultrafast Endocytosis.
1000 *Neuron*. 98:1184-1197 e1186.

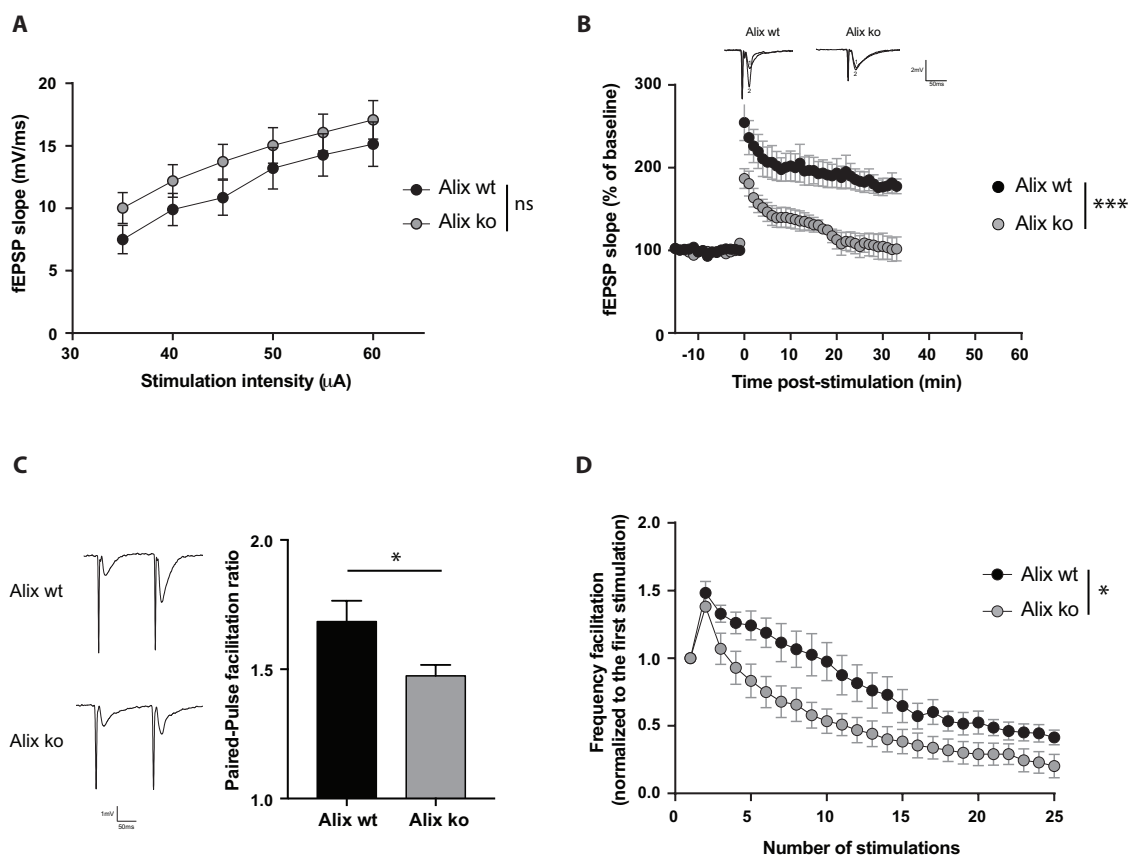
1001
1002

1003

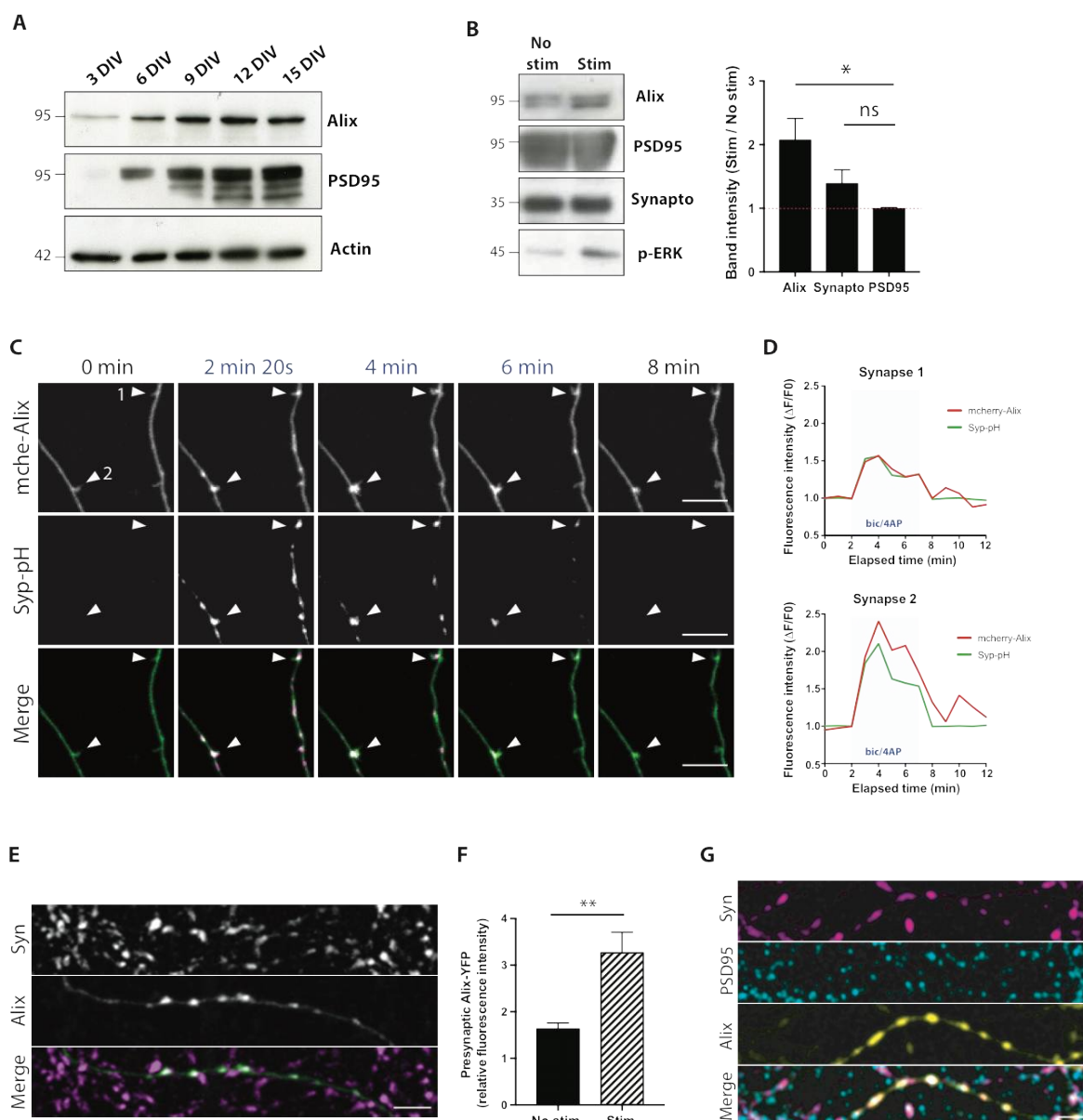


1004
1005
1006
1007
1008
1009
1010
1011
1012
1013
1014
1015
1016
1017

Figure 1. Alix is required for synaptic organisation. A, B) show no apparent effect of the lack of Alix on the number of synapses both in vivo or in vitro. A) Representative electron micrographs of the CA1 stratum radiatum from Alix wt and ko brains. Presynaptic profiles are highlighted in blue, and dendritic spines are in purple (scale bar: 2 μm). Graph shows the synaptic density per μm^2 (n=3 animals per genotype, p=0.1395, Unpaired t test). B) 15 DIV hippocampal neurons were stained by dual immunofluorescence with anti-PSD95 and anti-synapsin-1 antibodies. Immunolabelled objects were considered synapses when both stainings were juxtaposed (scale bar: 10 μm). The graph represents the number of synapses per μm^2 (n=7 experiments, p=0.5501, Unpaired t test). C-G) Anomalies can be detected in synapses of Alix ko brains. C, F) Representative electron micrographs of CA1 from Alix wt and ko mice (scale bar: 200 nm). Graphs represent D) numbers of synaptic vesicles per μm^2 (n=136 synapses from 3 animals, p=0.0009, Mann Whitney test), E) presynaptic bouton surface area (n=136 synapses from 3 animals, p=0.0036, Mann Whitney test), G) PSD length (n=136 synapses from 3 animals, p=0.0001, Mann Whitney test) and H) ratio between the diameter of the spine head and neck.

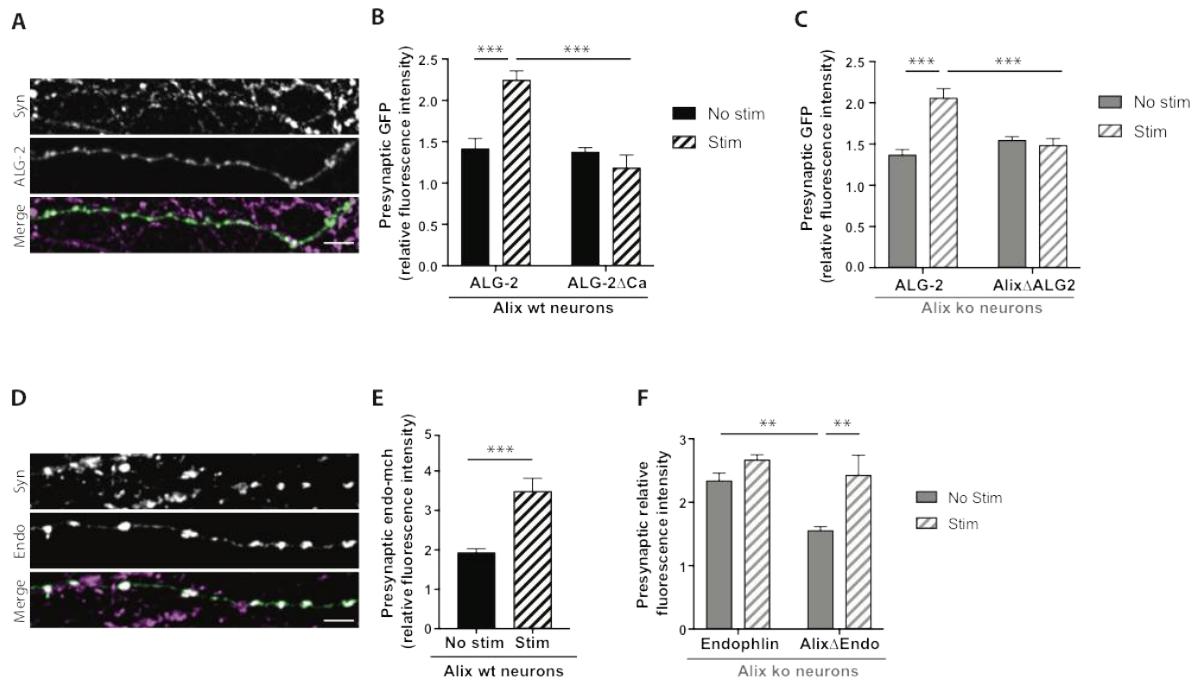


1018
 1019 **Figure 2. Synaptic plasticity in CA1 is altered in absence of Alix.** A) Input-output relationship of fEPSP
 1020 slope evoked by stimulation of Schaeffer collaterals at various intensities in slices from Alix wt and ko
 1021 mice (n=16 wt slices and n=13 ko slices from 3 animals per genotype, p=0.9166, two-way ANOVA). B)
 1022 Long-term potentiation of fEPSP slope evoked by high frequency stimulation of Schaeffer collaterals
 1023 delivered at time 0. Inserts show representative EPSPs traces. (n=5 slices from 3 animals per genotype,
 1024 p=0.0001, two-way ANOVA). C) Paired-pulse facilitation ratio. Facilitation is induced by two
 1025 consecutive stimuli of Schaeffer collaterals separated by 50 ms (n=16 wt slices and n=13 ko slices from
 1026 3 animals per genotype, p=0.0187, Unpaired t test). Representative traces are shown on the left. D)
 1027 Synaptic fatigue induced by stimulation of Schaffer collaterals at 25 Hz (n=5 slices from 3 animals per
 1028 genotype, p=0.0001, two-way ANOVA). (n=136 synapses from 3 animals, p=0.0001, Mann Whitney
 1029 test).
 1030

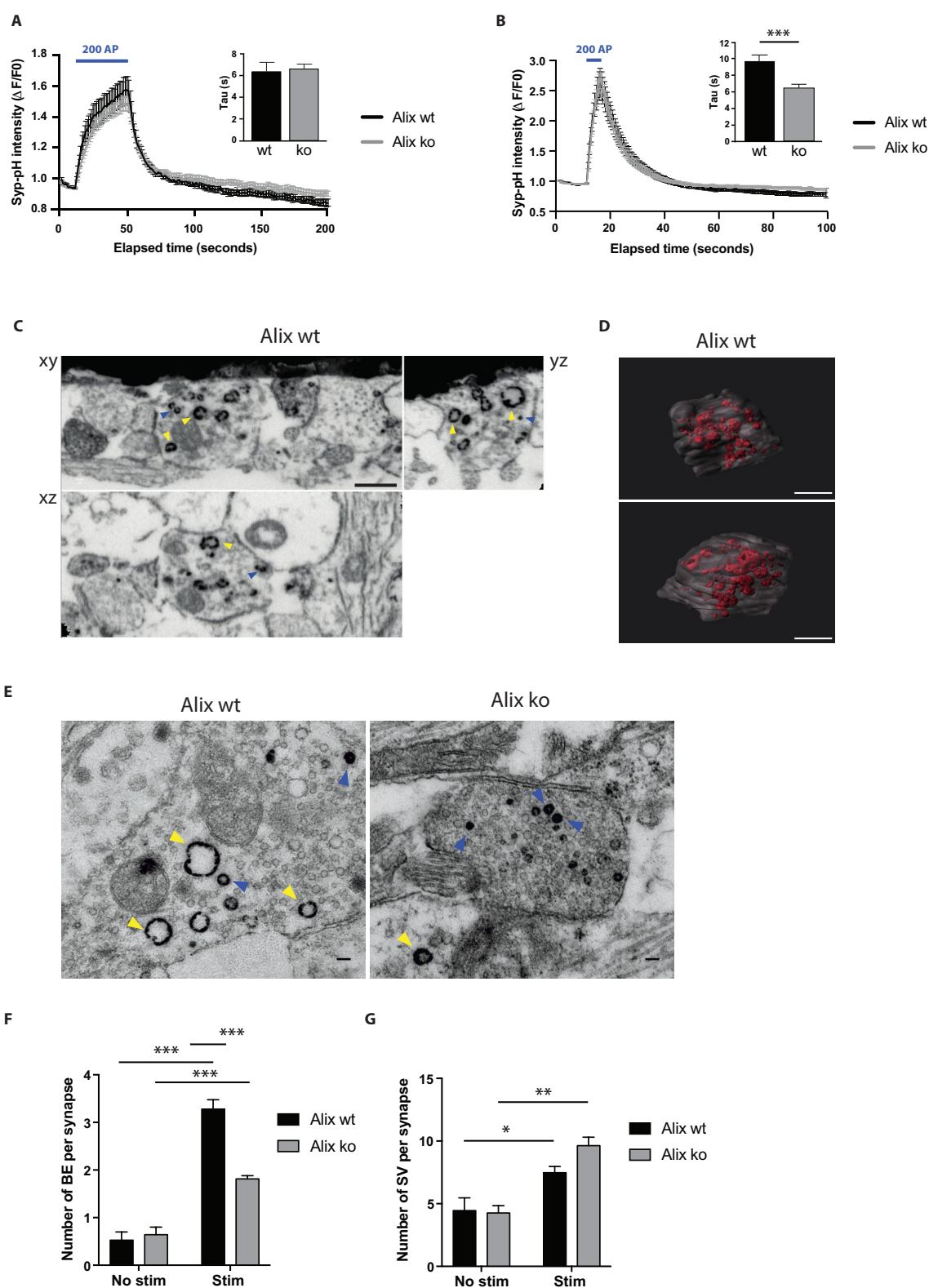


1031
 1032 **Figure 3. Alix is recruited presynaptically during synaptic activation.** A) Western blot showing Alix
 1033 expression during neuronal maturation in cortical cultures. PSD95 expression was used to monitor
 1034 synaptogenesis with time in culture. B) Western blot showing increase of Alix in synaptosome-enriched
 1035 neuronal membranes upon neuronal stimulation by bicuculline/4AP. Synaptophysin and PSD95 were
 1036 used as pre- and postsynaptic markers, respectively. The phosphorylated form of ERK (p-ERK) was used
 1037 to assess the efficiency of the stimulation. (n=4 experiments, Alix versus PSD95, p=0.0187, one-way
 1038 ANOVA). C) Images from time-lapse video microscopy of 15 DIV hippocampal neurons expressing
 1039 mCherry-Alix (mche-Alix) and synaptophysin-pHluorin (Syp-pH). White arrowheads indicate
 1040 presynaptic boutons where Alix is recruited during a 5 min bicuculline/4AP stimulation starting at 2
 1041 min (images at 2:20, 4 and 6 min) (scale bar: 10 μm). D) Profile of mche-Alix recruitment to presynaptic
 1042 boutons 1 and 2 of figure 3C and the corresponding Syp-pH profile. Blue box indicates the
 1043 bicuculline/4AP incubation. E, F) 15 DIV hippocampal neurons expressing Alix-YFP (green) stimulated
 1044 for 5 min, fixed and presynaptic boutons revealed with anti-synapsin-1 antibody (Syn, magenta) (scale
 1045 bar: 5 μm). Graph shows the presynaptic increase in Alix-YFP upon stimulation. Presynaptic Alix-YFP
 1046 corresponds to the ratio of YFP fluorescence between synapsin-positive and -negative axonal regions
 1047 (n=12 neurons per condition from 4 experiments, p=0.0017, Unpaired t test). G) 15 DIV hippocampal
 1048 neurons expressing Alix-YFP (yellow), stimulated for 5 min, fixed and stained with anti-PSD95 (cyan)

1049 for postsynaptic densities and anti-synapsin-1 (magenta) (scale bar: 5 μ m).



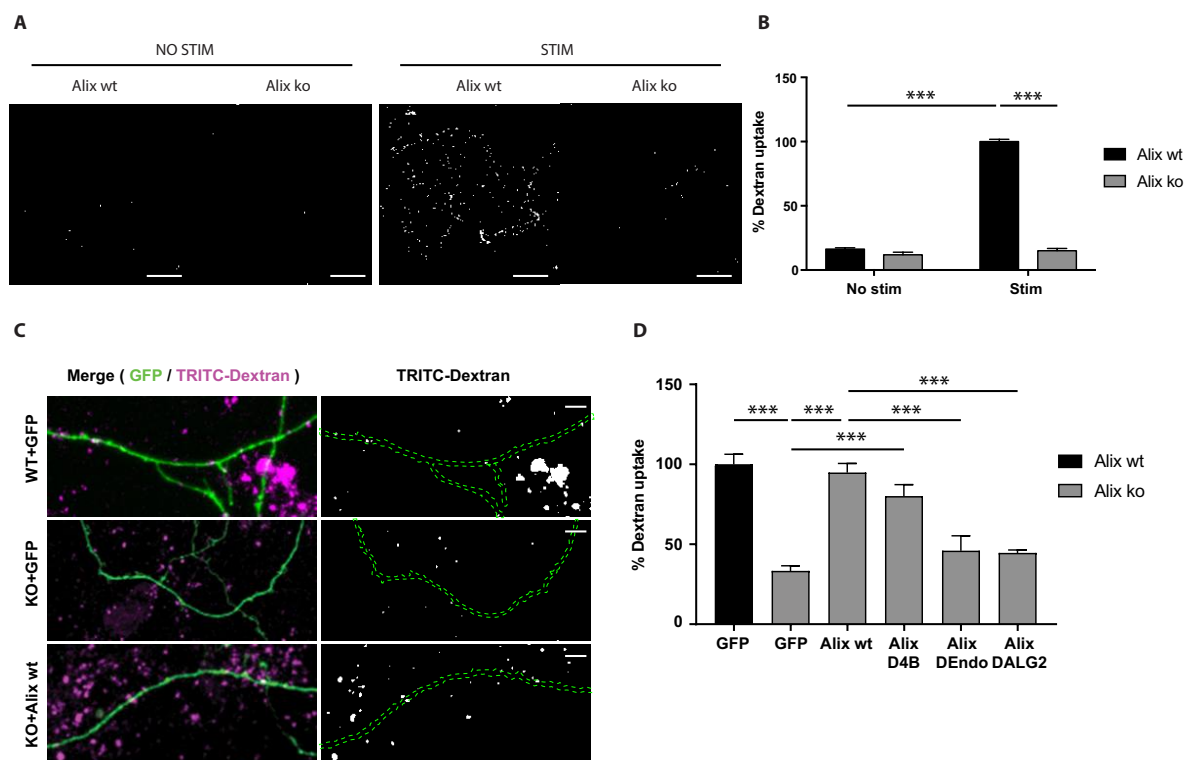
1050
1051 **Figure 4. Interplay between Alix, ALG-2 and endophilin recruitments at activated synapses.** All
1052 experiments made use of 15 DIV hippocampal neurons expressing the indicated constructs. Neurons
1053 were stimulated with bicuculline/4AP for 5 min before fixation and staining with antisynapsin-1. A)
1054 GFP-ALG-2 (green) is recruited presynaptically (scale bar: 5 μ m). B) Quantification of synaptic
1055 recruitments of GFP-ALG-2 and GFP-ALG2 Δ Ca in Alix wt neurons shows that ALG-2 presynaptic increase
1056 depends on its capacity to bind calcium (n=10 and n=7 neurons for GFP-ALG2 stimulated and not
1057 stimulated, respectively and n=6 and n=12 neurons for GFP-ALG2 Δ Ca stimulated and not stimulated,
1058 respectively, in 3 experiments, p=0.0001, one-way ANOVA). C) In Alix ko neurons GFP-ALG2 is recruited
1059 pre-synaptically but GFP-Alix Δ ALG2 is not recruited indicating that Alix recruitment depends on its
1060 capacity to bind ALG-2 (n=17 neurons for both GFP-ALG2 stimulated and not stimulated, and n=15 and
1061 n=18 neurons for GFP-Alix Δ ALG2 stimulated and not stimulated, respectively, from at least 3
1062 experiments, p=0.0001, one-way ANOVA). D, E) endophilin-mCherry (green) concentrates at
1063 presynaptic parts of stimulated wt, but not Alix ko, neurons (scale bar: 5 μ m) (n=12 and n=10 neurons
1064 for stimulated and not stimulated, respectively from 3 experiments, p=0.0001, Mann Whitney test). F)
1065 Alix recruitment does not depend on its binding to endophilins as shown using GFP-Alix Δ Endo in Alix
1066 ko neurons (n=15 and n=13 neurons for endophilin-mCherry stimulated and not stimulated,
1067 respectively, and n=9 and n=10 neurons for GFP-Alix Δ Endo stimulated and not stimulated, respectively,
1068 from 3 experiments p=0.0031, one-way ANOVA).
1069



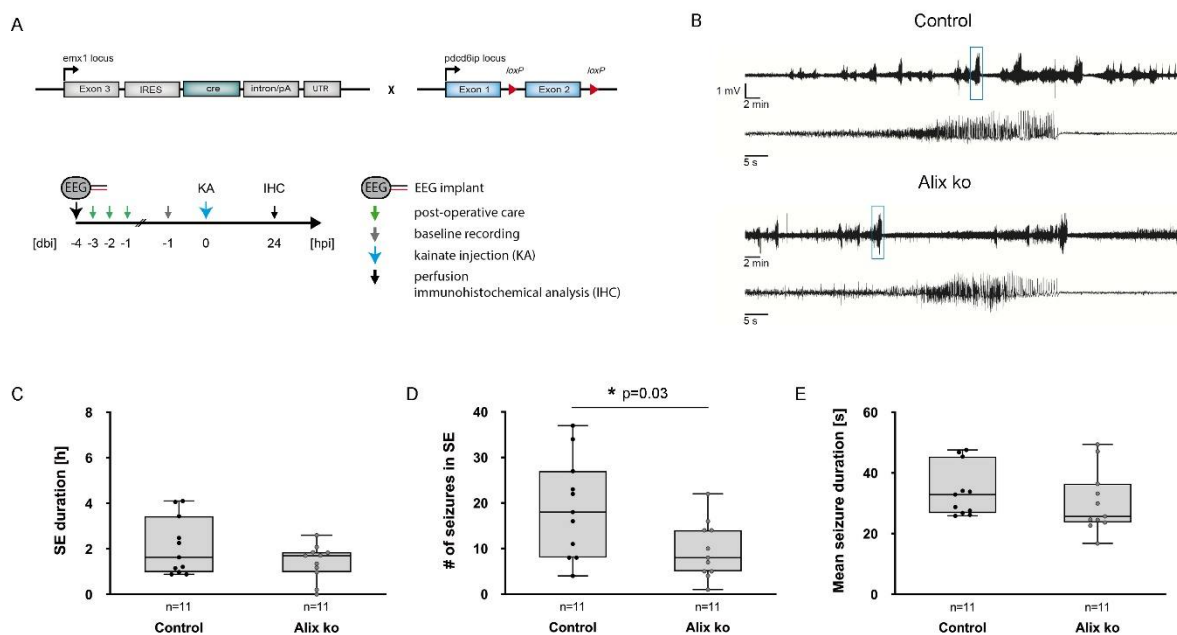
1070
1071
1072
1073
1074

Figure 5. Alix is necessary for activity-dependent bulk endocytosis. A, B) Average traces of Syp-pH fluorescence in synaptic boutons of Alix wt and ko hippocampal neurons stimulated with 200 action potentials (AP) applied at 5 Hz (A) or 40 Hz (B) (16-46 fields of view per condition from 4 experiments for wt and 5 for ko mice). Insets show the exponential fit of fluorescence decay after stimulations in

1075 the fields imaged. (A) $p = 0.99$; (B) $p = 0.001$ one-way ANOVA. C, E) Electron micrographs of cerebellar
1076 granule neurons stimulated in presence of free HRP to label newly-formed synaptic vesicle (blue
1077 arrowhead) and bulk endosomes (yellow arrowhead). C) Focused ion beam scanning electron
1078 microscopy (FIB-SEM); orthogonal views from different planes (xy, xz or yz) extracted from a stack used
1079 for the 3D reconstruction of WT pre-synaptic terminal shown in D). Scale bar: 500nm. D) Two different
1080 views of the reconstructed synapse are shown where the membrane is represented in transparent
1081 gray and HRP-positive structures in red (Scale bar: 500nm). E, F, G) transmission electron microscopy
1082 of HRP incubated CB neurons was used to quantify the number of bulk endosomes (F) and synaptic
1083 vesicles (G) in Alix wt and ko cerebellar neurons (F, $n=4$ experiments, $p=0.0008$, one-way ANOVA) or
1084 synaptic vesicles (G, $n=4$ experiments, $p=0.0393$ one-way ANOVA). (E, scale bar: 100 nm).
1085

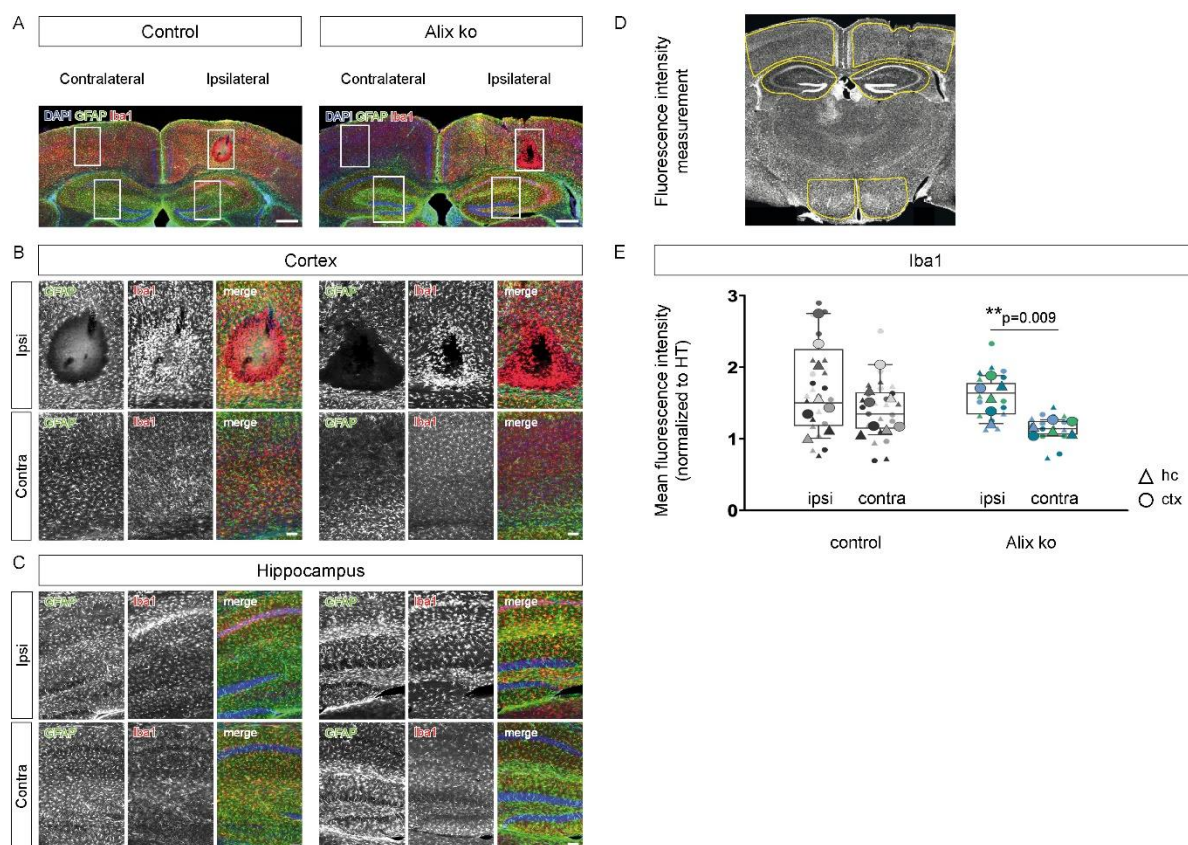


1086
1087 **Figure 6. Alix binding to Alg-2 and endophilin but not CHMP4 is essential for bulk endocytosis.** A, B)
1088 Dextran uptake is triggered by Bicuculline/4AP stimulation in Alix wt, but not in Alix ko, neurons.
1089 Confocal images of Alix wt and Alix ko hippocampal neurons stimulated in the presence of 10kDa
1090 dextran (scale bar: 50 μ m) (n=4 experiments, p=0.0001, one-way ANOVA). C) Representative images
1091 of Dextran uptake by Alix wt neurons (top), Alix ko neurons expressing GFP (middle), or Alix ko neurons
1092 expressing GFP and Alix (bottom). D) Dextran uptake is rescued in Alix ko neurons expressing Alix wt
1093 and Alix Δ Chmp4B (Alix Δ 4B), but not Alix Δ ALG2 or Alix Δ endo. % of dextran uptake corresponds to the
1094 number of dextran spots per μ m expressed as percentages of the positive control for each experiment
1095 (n=17 neurons for wt neurons, n=13 neurons for ko+GFP, n=11 for ko+Alix, n=12 neurons for
1096 ko+Alix Δ endo, n=12 for ko+Alix Δ Chmp4B, and n=11 for ko+Alix Δ ALG2, all from at least 3 experiments,
1097 p=0.0001, one-way ANOVA).



1098
1099

1100 **Figure 7 Alix ko mice develop less seizures during status epilepticus.** A) $Emx1^{IREScre}$ (Emx-Cre) and
 1101 $Alix^{fl/fl}$ mouse lines were crossbred to delete Alix in neocortical and hippocampal excitatory neurons
 1102 (Alix ko). Animals were implanted with telemetric EEG transmitters to assess seizure activity. EEG
 1103 recording started one hour before *status epilepticus* (SE) induction via intracortical kainate (KA)
 1104 injection and ended 24 hours post KA. Subsequently, the brains were processed for
 1105 immunohistochemical staining. B) Representative EEG traces from Emx-Cre control and Alix ko animals.
 1106 C) Total duration of SE did not differ between Alix ko and Emx-Cre control mice ($p=0.49$). D) Alix ko
 1107 animals experience about 66 % less seizures during SE than Emx-Cre controls ($*p=0.03$). E) Mean
 1108 seizure duration during SE was not affected in Alix ko mice compared to Emx-Cre controls ($p=0.19$).
 1109 N (control) = 11 animals, n (Alix ko) = 11 animals. Statistical analysis was performed with the Mann-
 1110 Whitney test, $*p<0.05$.
 1111



1112
1113
1114
1115
1116
1117
1118
1119
1120
1121
1122
1123
1124
1125
1126
1127
1128
1129
1130
1131

Figure 8 Reduced contralateral activation of microglia in Alix ko mice suggests reduced (contralateral) propagation of epileptiform activity. A) Coronal overviews of brain slices 24Scale bar= 500 μ m. B) Magnification of highlighted cortical areas in (A) show an increased ipsilateral (ipsi) microglial activation (Iba1) compared to contralateral (contra), which was more pronounced in Alix ko mice. Astroglial reactivity (GFAP) was moderately increased adjacent to the injection site in both groups. Scale bar= 100 μ m. C) Magnification of highlighted hippocampal areas in (A). Contralateral hippocampi of Alix ko mice displayed reduced microglial activation (Iba1) relative to the ipsilateral side, which was less apparent in control mice. Astroglial reactivity (GFAP) was comparable in hippocampi of control and Alix ko mice. Scale bar= 100 μ m. D) Depiction of fluorescence intensity measurement areas in cortex, hippocampus and hypothalamus. E) In Alix ko mice, the contralateral Iba1 immunoreactivity was about 30 % reduced in comparison to ipsilateral (**p= 0.009), in contrast to control mice (p= 0.645). Circles and triangles represent individual quantifications from cortex and hippocampus, respectively. One data point corresponds to the average of three slices from the same animal. Red and black symbols indicate ipsi- and contralateral sides. Fluorescence intensity values were normalized to the hypothalamic area (HT) of the respective hemisphere. N (control) = 4 animals, n (Alix ko) = 3 animals. Statistical analysis was performed on the average value of three slices per animal, with the Mann-Whitney test, *p< 0.05, **p <0.01.